nature cancer

Article

https://doi.org/10.1038/s43018-025-01009-x

CAR-engineered lymphocyte persistence is governed by a FAS ligand–FAS autoregulatory circuit

Received: 23 February 2024

Accepted: 2 June 2025

Published online: 22 July 2025

Check for updates

Fei Yi[1], Tal Cohen[1,2], Natalie Zimmerman[1], Friederike Dündar[3,4,5], Paul Zumbo[3,4], Razan Eltilib[1], Erica J. Brophy[1], Hannah Arkin[1], Judith Feucht[6,7], Michael V. Gormally[1,8], Christopher S. Hackett[9], Korbinian N. Kropp[1], Inaki Etxeberria[1], Smita S. Chandran[1], Zeguo Zhao[6,10], Winson Cai[11], Anthony F. Daniyan[8,9,12], Jae H. Park[6,8,9,12], Caleb A. Lareau[13], Katharine C. Hsu[1,6,9,14,15], Michel Sadelain[6,10], Doron Betel[4,9,16] & Christopher A. Klebanoff[1,6,8,9,17]

Chimeric antigen receptor (CAR)-engineered lymphocytes treat B cell malignancies; however, limited persistence can restrain the full therapeutic potential of this approach. FAS ligand (FAS-L)/FAS interactions govern lymphocyte homeostasis. Knowledge of which cells express FAS-L in patients with cancer and whether these sources compromise CAR persistence remains incomplete. Here, we constructed a single-cell atlas of diverse cancers to identify cellular subsets expressing *FASLG*, the gene encoding FAS-L. We discovered that *FASLG* expression is limited primarily to endogenous T cells, natural killer (NK) cells and CAR-T cells, while tumor and stromal cell expression is minimal. To establish whether CAR-T and CAR-NK cell survival is FAS-L regulated, we performed competitive fitness assays using FAS-dominant negative receptor (ΔFAS)-modified lymphocytes. Following transfer, ΔFAS-expressing CAR-T/CAR-NK cells became enriched, a phenomenon that mechanistically was reverted through *FASLG* knockout. By contrast, *FASLG* was dispensable for CAR-mediated tumor killing. In multiple models in female mice, ΔFAS coexpression enhanced antitumor efficacy. Together, these findings reveal that CAR-engineered lymphocyte persistence is governed by a FAS-L/FAS autoregulatory circuit.

CAR-T cell therapies have revolutionized the treatment of B cell malignancies[1,2] and are now showing early signs of efficacy in solid cancers[3–9]. Despite ongoing progress, many patients who receive CAR therapies fail to respond or develop resistance, highlighting a critical need to further optimize current treatments. Multiple factors may contribute to disease progression following CAR treatment, which can be categorized as tumor-intrinsic, tumor microenvironment or lymphocyte-intrinsic resistance mechanisms[10]. Among these, factors associated with CAR-expressing lymphocytes are of particular interest because they are potentially modifiable during ex vivo cell manufacturing. Across clinical studies, the in vivo expansion and persistence of CAR-T cells is frequently associated with superior outcomes[11–15]. Recent clinical data indicates that this holds true not only for CAR-T cells but also CAR-modified NK cells (CAR-NK)[16], a lymphocyte subset with desirable features for allogeneic applications[17]. Thus, enhancing the survivability of CAR-T and CAR-NK cells remains a major goal in the cell therapy field.

Genome-wide[18,19] and focused[20–22] CRISPR screens have recently identified *FAS* as a major determinant of antitumor T cell persistence

A full list of affiliations appears at the end of the paper. e-mail: klebanoc@mskcc.org

https://doi.org/10.1038/s43018-025-01009-x

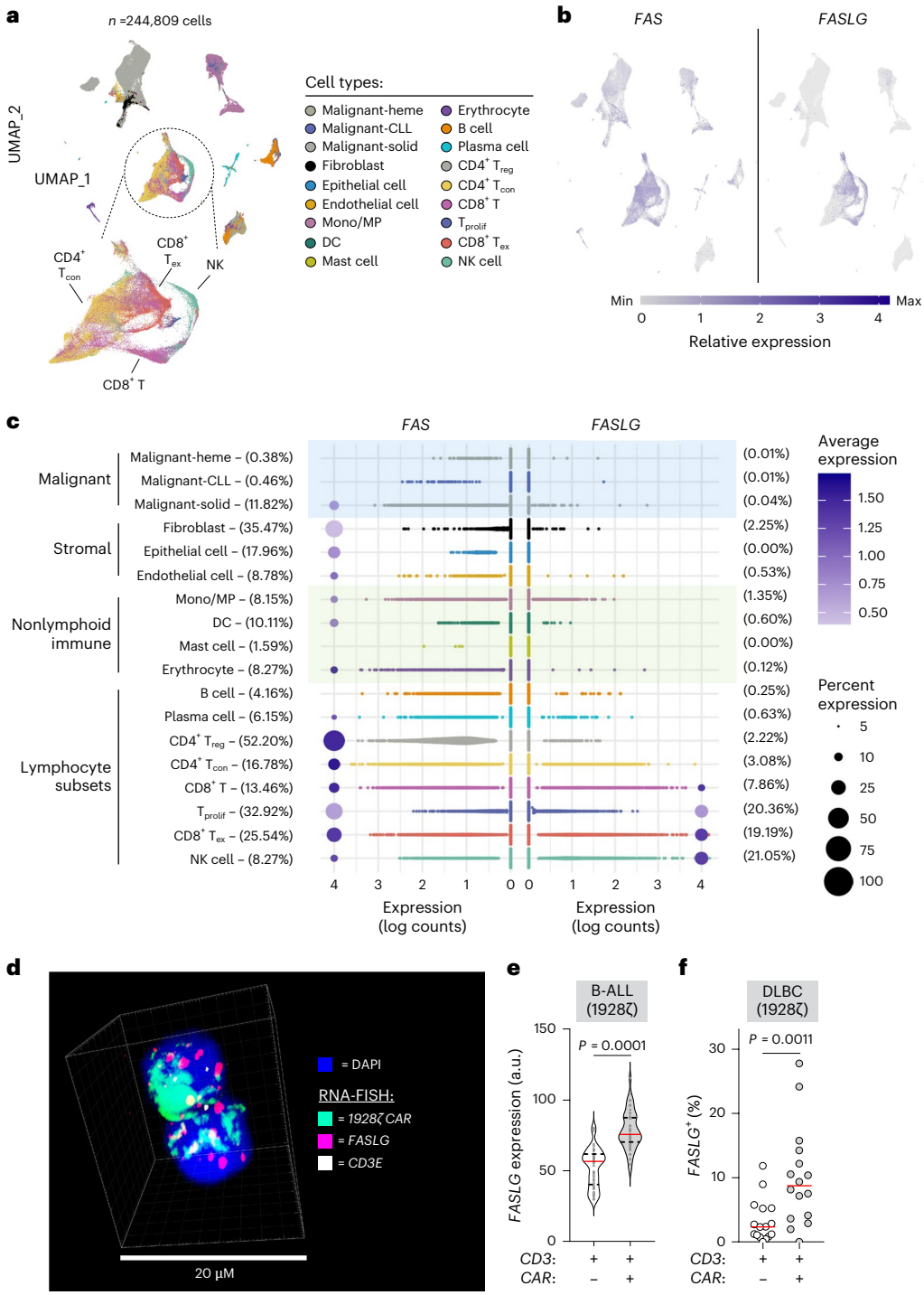

Fig. 1 | *FASLG* is expressed by endogenous and CAR-expressing lymphocytes. **a**, UMAP visualization of scRNA-seq from $n = 244,809$ immune and nonimmune cells obtained from the tumor and peripheral blood of patients with $n = 10$ hematologic cancers, $n = 27$ solid cancers and peripheral blood from $n = 4$ healthy donors. Each dot represents an individual cell assigned to one of 18 inferred cell types. CLL, chronic lymphocytic leukemia; Mono, monocyte; MP, macrophage; DC, dendritic cell; T_{reg}, regulatory T cell; T_{con}, conventional T cell; T_{prolif}, proliferating T cell. **b**, Log-transformed normalized gene expression values for *FAS* and *FASLG* overlaid on the UMAP coordinates defined in **a**. **c**, Comparison of the frequency and magnitude of *FAS* and *FASLG* expression by individual cells assigned to each inferred cell type identified in the UMAP. Bubble size represents the frequency of each cell type that expresses the indicated gene and color indicates the relative intensity of expression. **d**,**e**, Representative immunofluorescent confocal image (**d**) and summary violin plots (**e**) quantifying *FASLG* mRNA expression by endogenous and CAR-expressing T cells in the bone marrow of patients with B-ALL treated with a 1928ζ CAR. Samples were co-hybridized with DAPI (blue) and multiplexed RNA-FISH probes specific for the mRNA sequence of the CAR's single-chain variable fragment (scFv) (green), *CD3E* mRNA (white) and *FASLG* mRNA (red). Data are derived from 52 annotated regions using samples from $n = 3$ patients. Violin distributions are centered around the median (red horizontal line) with quartiles ranges displayed above and below (dashed horizontal lines). The maxima and minima are represented by the top and bottom of each plot. Each dot represents mean *FASLG* mRNA expression within a particular cell type from an annotated region of interest. **f**, Summary scatter-plot demonstrating the frequency of $FASLG^+$ T cells which either coexpress or do not express a 1928ζ CAR transgene in $n = 16$ patients with diffuse large B cell lymphoma (DLBC) measured using scRNA-seq. Each dot represents an individual patient. All *P* values were calculated using a two-sided Student's *t*-test. a.u., arbitrary fluorescence units.

under chronic antigen stimulation conditions. FAS is one of five tumor necrosis factor (TNF) superfamily death receptors that induces caspase-dependent apoptosis following engagement with an extracellular ligand[23]. These findings provide a strong rationale for disabling FAS signaling in receptor engineered T cells[19–21,24–28]; however, while the role of FAS in regulating naturally occurring T cell homeostasis is well established, whether this pathway governs CAR-T and CAR-NK longevity remains unknown. Moreover, the dominant cellular sources of FAS-L in patients with cancer remain incompletely defined. Here, we aimed to address three critical gaps in knowledge regarding the immunobiology of FAS in the context of CAR-based therapies. First, we sought to define which cells express *FASLG* in patients. Second, we sought to establish whether CAR-engineered lymphocyte persistence is negatively self-regulated by *FASLG*. Finally, we sought to determine whether *FASLG* is required for on-target CAR-T and CAR-NK effector functions against B cell malignancies. Our findings reveal that CAR-engineered lymphocyte persistence is governed by a FAS-L/FAS autoregulatory circuit. Thus, disruption of FAS signaling can serve as a generalizable strategy to enhance the therapeutic potency of genetically engineered T cells and NK cells.

Results

FASLG is expressed by endogenous and CAR$^+$ lymphocytes

We previously reported that ~73% of cancer types represented in The Cancer Genome Atlas overexpress *FASLG*, the gene encoding FAS-L, compared to matched healthy tissues[24]. When analyzed on a patient-level basis, we found a strong positive correlation between expression of lineage-defining T and NK cell genes and *FASLG* (Extended Data Fig. 1). This finding held true across inflamed and noninflamed histotypes, suggesting that activated lymphocytes might be the primary source of *FASLG* within the tumor microenvironment; however, because these associations were made using bulk RNA sequencing (RNA-seq), the identity of specific ligand-expressing cell type(s) could not be resolved unambiguously. To precisely define which cellular subsets express *FASLG*, we generated an integrated human single-cell transcriptomic atlas consisting of 244,809 immune and nonimmune cells using publicly available datasets (Extended Data Fig. 2). To capture phenotypic heterogeneity, cells were interrogated from 37 patients with cancer and four healthy donors. After applying stringent quality controls and a standardized analysis pipeline, Uniform Manifold Approximation and Projection (UMAP) visualization revealed nine distinct clusters (Fig. 1a). Expression of canonical marker genes identified 18 major cell types that were subcategorized as malignant, stromal, nonlymphoid immune and lymphocyte subsets. Overlay of messenger RNA expression for specific genes onto the UMAP coordinates revealed that *FAS* was broadly distributed across many cell types (Fig. 1b,c). By contrast, *FASLG* expression was highly restricted and limited primarily to T and NK cells. In this analysis, there was minimal to no *FASLG* expression by malignant and stromal cells.

Having resolved the landscape of *FASLG* expression by endogenous cells, we next sought to measure expression by CAR-T cells in patients. We developed and validated a multiplexed fluorescent RNA in situ hybridization (RNA-FISH) assay to quantify coexpression of mRNA for a 1928ζ CAR transgene, *CD3E* and *FASLG* at single-cell resolution (Extended Data Fig. 3). Using bone marrow biopsy samples from patients with B cell acute lymphoblastic leukemia (B-ALL) treated in the context of a clinical trial (NCT01044069)[11], we found that CAR-T cells consistently expressed significantly higher levels of *FASLG* compared to endogenous T cells (Fig. 1d,e). We confirmed the generalizability of this finding by analyzing single-cell RNA-seq (scRNA-seq) data from patients with diffuse large B cell lymphoma who received CAR-T cells[29]. Here also, *FASLG* expression was significantly higher in CAR-expressing compared to nonmodified T cells (Fig. 1f). We conclude that *FASLG* expression is highly restricted within patients with cancer and primarily associated with endogenous lymphocytes and CAR-modified T cells.

CAR-T derived *FASLG* regulates cellular persistence in vivo

We hypothesized that FAS-L expression by CAR-T cells engages FAS$^+$CAR-T cells to induce apoptosis and limit cellular persistence. To test this, we performed competitive fitness assays using phenotypically discernable populations of human CAR-T cells that are either responsive or unresponsive to FAS signaling (Fig. 2a). T cells were transduced with one of two multi-cistronic vectors: (1) a vector encoding a 1928ζ CAR, a FAS-dominant negative receptor (ΔFAS) and truncated epidermal growth factor receptor (tEGFR); or (2) a vector encoding an identical CAR and truncated low-affinity neuronal growth factor (tLNGFR). tEGFR and tLNGFR are nonfunctional cell surface molecules that enable mixed cell populations to be tracked longitudinally[30,31]. Our rationale for coexpressing ΔFAS alongside a CAR was threefold. First, ΔFAS is highly efficient at disrupting endogenous FAS function[32]. Second, coexpression helps ensure that measured differences in the numbers of CAR-expressing lymphocytes is attributable to the cell-intrinsic effect of disrupting FAS signaling[33]. Third, it avoids the potential for artifact resulting from chromosome loss, a phenomenon reported for CRISPR/Cas9-mediated gene knockout (KO) in T cells[34]. We confirmed that ΔFAS blocks FAS-L-induced T cell apoptosis and has no detrimental impact on antigen-dependent effector functions (Fig. 2b–d). Further, we found that ΔFAS reduces caspase 3/7 activation in resting CAR-T cells, a finding that correlates with the capacity of the 1928ζ CAR to induce low-level tonic signaling (Fig. 2e,f). Finally, we discovered that ΔFAS protects against TCR-dependent elimination of allogeneic lymphocytes (Fig. 2g,h and Extended Data Fig. 4), a feature that may facilitate engraftment in human leukocyte antigen (HLA) mismatched hosts.

Fig. 2 | Cell-intrinsic disruption of FAS signaling blocks CAR-T cell apoptosis and protects against TCR-mediated rejection of allogeneic lymphocytes. **a**, Schematic of multi-cistronic vectors encoding tEGFR and a 1928ζ CAR alone (EC) ± a FAS-dominant negative receptor (ΔFAS) (ECF). **b**, Representative FACS plots for activated caspase 3/7 in human T cells left untransduced (UT) or transduced with an indicated vector. Caspase activity was measured at rest and 4 h following stimulation with 100 ng ml^{-1} of a recombinant FAS-L molecule (lzFAS-L). Median of $n = 3$ biologically independent samples is shown with mean ± s.e.m. of gated activate caspase 3/7$^+$ lymphocytes. **c**, Simplified Presentation of Incredibly Complex Evaluations (SPICE) analysis representing cytokine polyfunctionality of T cells transduced with indicated CAR constructs and co-cultured with or without K562-CD19 cells. T cells exposed to PMA/I were used as a positive control. Concentric plots indicate the median expression of indicated cytokines from $n = 3$ biologically independent samples. **d**, Cytolytic activity of UT, EC or ECF-expressing T cells against Nalm6/mCherry. Data are shown as mean ± s.e.m. using $n = 3$ biologically independent samples. *P* values calculated using a one-way analysis of variance (ANOVA) with Welch's correction. **e**,**f**, Representative FACS plots (**e**) and summary scatter-plot (**f**) measuring ZsGreen expression by Jurkat NFAT-ZsGreen reporter cells transduced with tEGFR alone (E), EC or ECF ($n = 12$ biologically independent samples). As a positive control, an aliquot of transduced Jurkat cells were exposed to PMA/I ($n = 3$ biologically independent samples). Data are shown as mean ± s.e.m. *P* values were calculated using a one-way ANOVA with a Šídák's multiple comparisons test. **g**,**h**, Representative FACS plots (**g**) and summary graph (**h**) displaying the ratio of HLA-A*03:01$^+$ T cells transduced with tLNGFR-1928ζ or tEGFR-1928ζ-ΔFAS tLNGFR and co-cultured with an indicated murinized (m)TCR transduced HLA-A*03:01$^-$ T cell population. The anti-HLA-A*03 TCR recognizes HLA-A*03$^+$ cells in a peptide agnostic manner while the Flu and *PIK3CA* (H1047L) TCRs recognize an HLA-A*03:01-restricted viral peptide and neopeptide, respectively. FACS plots were pre-gated on live$^+$mTCR$^-$HLA-A3$^+$ cells. Data displayed as the mean ratio of tLNGFR/tEGFR HLA-A*03:01$^+$ T cells ± s.e.m. using $n = 3$ biologically independent samples. Groups were compared using a one-way ANOVA with Šídák's multiple comparisons test.

https://doi.org/10.1038/s43018-025-01009-x

After characterizing the influence of ΔFAS on CAR-T cell function, we evaluated the impact of ΔFAS on CAR-lymphocyte persistence. We combined tEGFR$^+$ and tLNGFR$^+$ T cells in a ~1:1 ratio and transferred the mixed population into NOD/SCID/γc$^{-/-}$ (NSG) mice bearing established Nalm6 B-ALL (Fig. 3a). At the time of transfer, tEGFR$^+$ and tLNGFR$^+$ T cells consisted of comparable frequencies of stem cell memory T (T_{SCM}) and central memory T (T_{CM}) cells, subsets associated with superior CAR-T persistence (Fig. 3b)[12,13]. After one month, we observed significant enrichment in ΔFAS-expressing T cells across multiple tissues (Fig. 3c,d). These results were unlikely to be attributable to a xenogeneic response as co-culture of human CAR-T cells with murine cells did not cause *FASLG* upregulation (Extended Data Fig. 5).

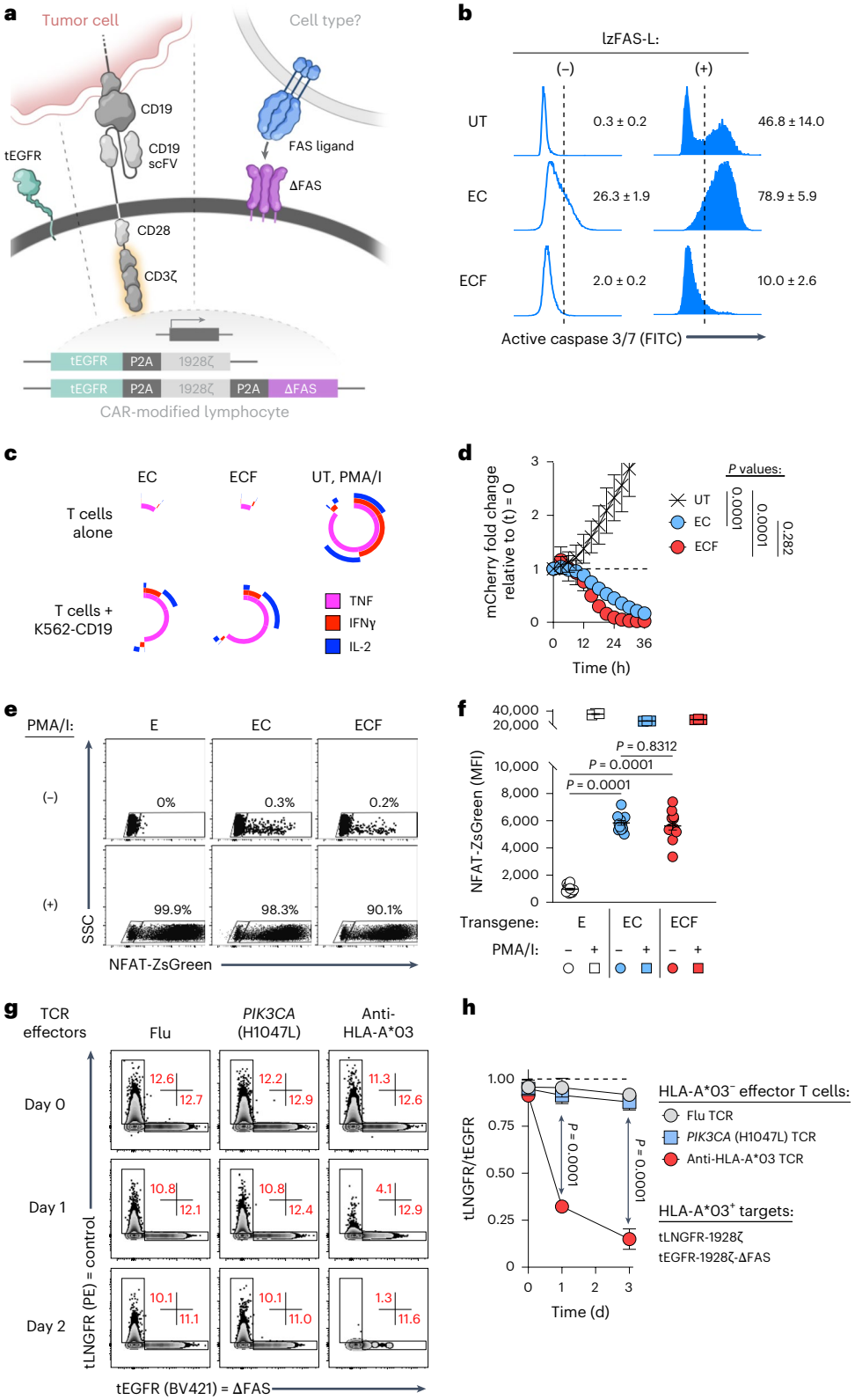

https://doi.org/10.1038/s43018-025-01009-x

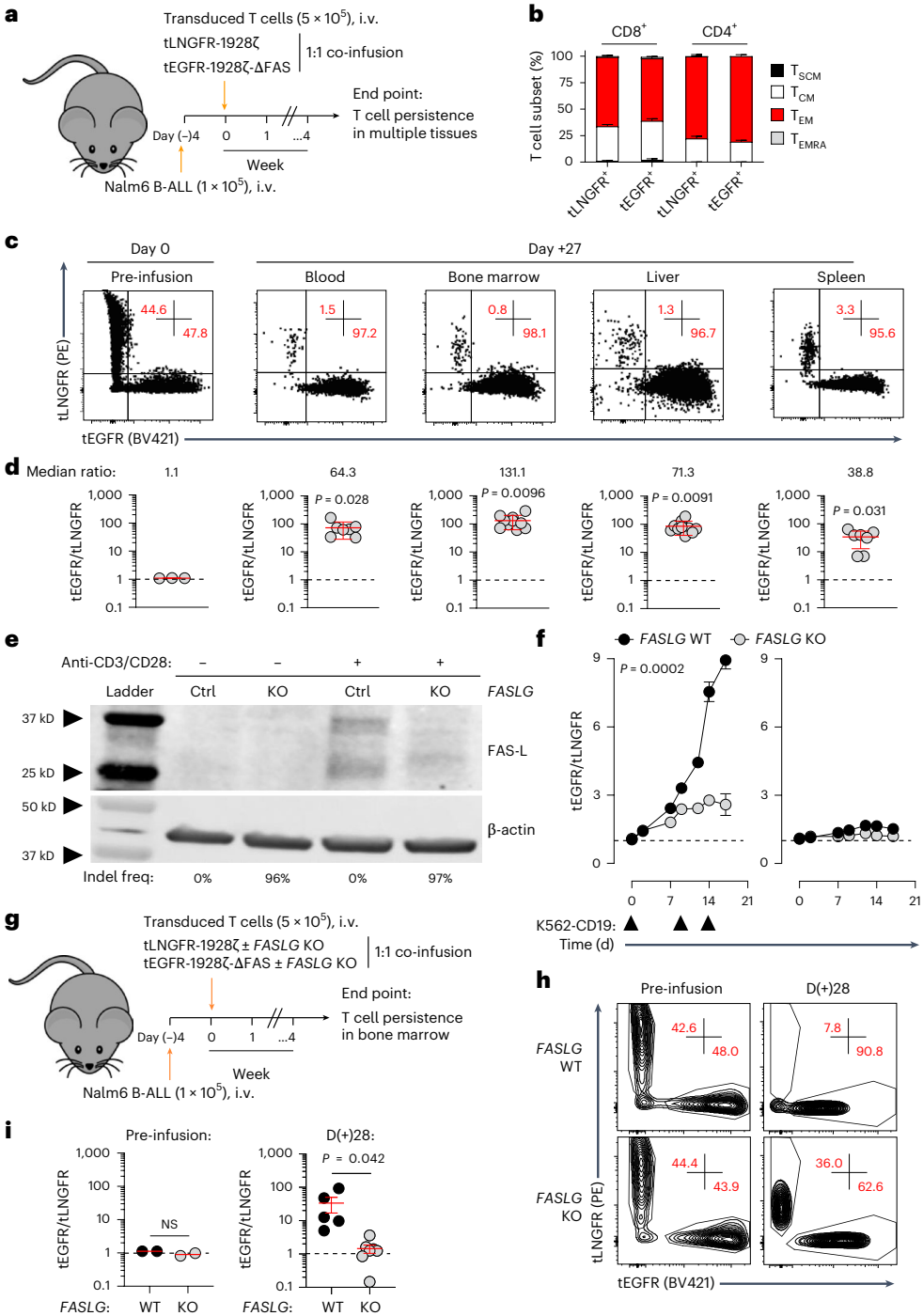

Fig. 3 | CAR-T derived *FASLG* auto-regulates cellular persistence in vivo. **a**, Experimental design to test persistence of T cells expressing a 1928ζ CAR ± ΔFAS in tumor-bearing mice. T cells were co-transferred into NSG mice bearing Nalm6 B-ALL and tracked based on tLNGFR or tEGFR expression. i.v., intravenous. **b**, Distribution of memory T cell subsets before transfer. Bar graphs displayed as mean ± s.e.m. using $n = 3$ biologically independent samples. T_{EM}, effector memory T cell; T_{EMRA}, terminal effector memory T cell. **c**,**d**, Representative FACS (**c**) and summary scatter-plots (**d**) measuring the ratio of tEGFR$^+$/tLNGFR$^+$ T cells at the time of infusion ($n = 3$ biologically independent samples) and following adoptive transfer. Symbols represent individually evaluated mice ($n = 10$) and are displayed as mean ± s.e.m. *P* values calculated based on comparison to the infusion product using a two-sided Student's *t*-test. **e**, Western blot for FAS-L protein from control or *FASLG* KO 1928ζ CAR-transduced T cells at rest or 48 h after anti-CD3/CD28 restimulation. The frequency of frameshift Indels in *FASLG* are displayed beneath each lane. Representative results from two independent experiments are shown. **f**, Relative antigen-driven in vitro expansion of control and *FASLG* KO 1928ζ CAR-T cells ± ΔFAS coexpression. CAR-T cells were combined ~1:1 and serially restimulated at indicated time points with K562-CD19 *FASLG* KO leukemia cells (left) or left unstimulated (right). Data are displayed as the mean ratio of tEGFR/tLNGFR T cells ± s.e.m. using $n = 3$ biologically independent samples. Groups compared using a paired two-tailed Student's *t*-test for accumulated differences between each time point. **g**, Experimental design to test the influence of CAR-T-derived *FASLG* on in vivo persistence in mice bearing established Nalm6 B-ALL. Control or *FASLG* KO tLNGFR-1928ζ CAR-T cells were co-transferred ~1:1 with control or *FASLG* KO tEGFR-1928ζ-ΔFAS CAR-T cells into Nalm6 B-ALL-bearing NSG mice. **h**,**i**, Representative FACS (**h**) and summary scatter-plot (**i**) comparing the ratio of tEGFR to tLNGFR cells at the time of infusion ($n = 2$ biologically independent samples) and 4 weeks following transfer. Symbols represent values from individually evaluated mice (*FASLG* wild-type (WT), $n = 5$; *FASLG* KO, $n = 7$) and are displayed as mean ± s.e.m. Groups were compared using a two-sided Student's *t*-test. NS, not significant ($P > 0.05$).

https://doi.org/10.1038/s43018-025-01009-x

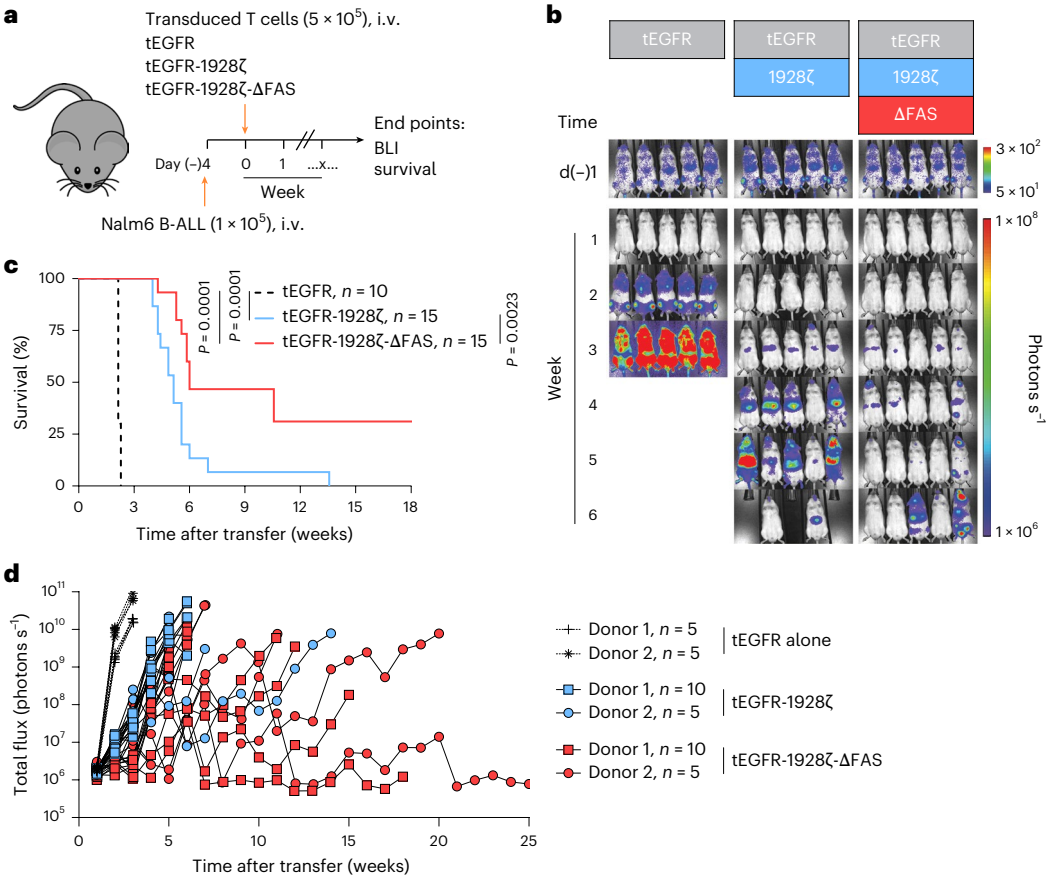

Fig. 4 | Disabling FAS signaling enhances CAR-T antitumor efficacy in vivo. **a**, Experimental design to compare the in vivo antitumor efficacy of human T cells that express a 1928ζ CAR ± a FAS-dominant negative receptor (ΔFAS) against established Nalm6-luciferase (Luc) B-ALL. **b**–**d**, BLI (**b**), overall survival curves (**c**) and quantification of tumor burden (**d**) for Nalm6-Luc B-ALL-bearing NSG mice treated by i.v. injection with 5×10^5 tEGFR$^+$ T cells transduced with an indicated vector. Pooled survival data from identically performed experiments using T cells from two unique donors is shown in **c** and is plotted as a Kaplan–Meier survival curve (tEGFR alone, $n = 10$; tEGFR-1928ζ, $n = 15$; tEGFR-1928ζ-ΔFAS, $n = 15$). Statistical comparisons were made using a log-rank test. Quantification of tumor burden as a function of time in mice treated with transduced T cells from an indicated donor measured using BLI (total flux) (**d**).

We next asked whether CAR-T cell-derived *FASLG* drives population skewing. To address this question, we ablated *FASLG* using CRISPR/Cas9-mediated gene knockout (KO). We confirmed a high frequency (>96%) of frameshift mutations at the *FASLG* locus in *FASLG* KO CAR-T cells. Multiple antibody clones failed to specifically detect FAS-L expression on human T cells using FACS (Extended Data Fig. 6). Therefore, to test whether FAS-L protein expression is activation dependent, we performed western blot on lysates from control and *FASLG* KO CAR-T cells at rest and after anti-CD3/CD28 stimulation. Minimal to no FAS-L was measured in resting CAR-T cells (Fig. 3e). After stimulation, two bands measuring ~37 kD and ~26 kD were detected in control-edited cells. These correspond to the integral membrane and metalloproteinase-generated soluble forms of FAS-L[35]. The presence of both bands was abrogated from activated *FASLG* KO cells, confirming gene disruption.

Having established that FAS-L expression by CAR-T cells is activation dependent, we tested the role of CAR-T cell-derived *FASLG* on cellular persistence. First, we measured the influence of repetitive in vitro stimulation using CD19$^+$K562 *FASLG* KO leukemia cells. In this experiment, ΔFAS/tEGFR-expressing CAR-T cells were added in a 1:1 ratio with tLNGFR-expressing control CAR-T cells. The mixed population was serially activated through addition of CD19$^+$K562 cells or left untreated as controls. The ratio of tEGFR/tLNGFR cells became progressively enriched for FAS signaling deficient CAR-T cells with each round of tumor stimulation (Fig. 3f). By contrast, the ratio of the two cell types remained close to one when *FASLG* KO CAR-T cells were used. Without stimulation, there were minimal differences between *FASLG* intact and KO cells and the ratio of tEGFR/tLNGFR remained stable over time. This indicates that disruption of FAS signaling in CAR-T cells does not lead to antigen-independent cell accumulation. Similar results were observed using T cells derived from a second healthy donor, using Nalm6 cells, and in two different solid tumor CAR-T models (Extended Data Fig. 7). Finally, we discovered that ΔFAS coexpression significantly delayed the acquisition of a terminally differentiated CAR-T cell phenotype (Extended Data Fig. 8). This latter finding was likely attributable to the generation of a progressively higher effector-to-target (E:T) ratio with each stimulation round, reducing the intensity of CAR-signaling on a per-cell basis.

Based on these findings in vitro, we sought to establish whether CAR-T cell-derived *FASLG* controls cellular persistence in vivo. To test this, T cells expressing tEGFR-1928ζ-ΔFAS and tLNGFR-1928ζ were recombined 1:1 after *FASLG* or control-KO (Fig. 3g). The mixed T cell population was infused into Nalm6 tumor-bearing mice and the ratio of tEGFR$^+$/tLNGFR$^+$ T cells was measured after 1 month. Consistent with our previous results, the balance of control-edited T cells became altered in favor of ΔFAS-expressing CAR-T cells. By contrast, the ratio of the two populations remained close to one with *FASLG* KO (Fig. 3h,i). We conclude that activation-induced FAS-L expression restrains the persistence of adoptively transferred CAR-T cells in a FAS-dependent manner.

Disabling FAS enhances CAR-T antitumor efficacy in vivo

Because FAS-L negatively regulated CAR-T cell persistence, we postulated that T cell-intrinsic disruption of FAS signaling would enhance CAR-dependent antitumor efficacy in vivo. To test this hypothesis, we

https://doi.org/10.1038/s43018-025-01009-x

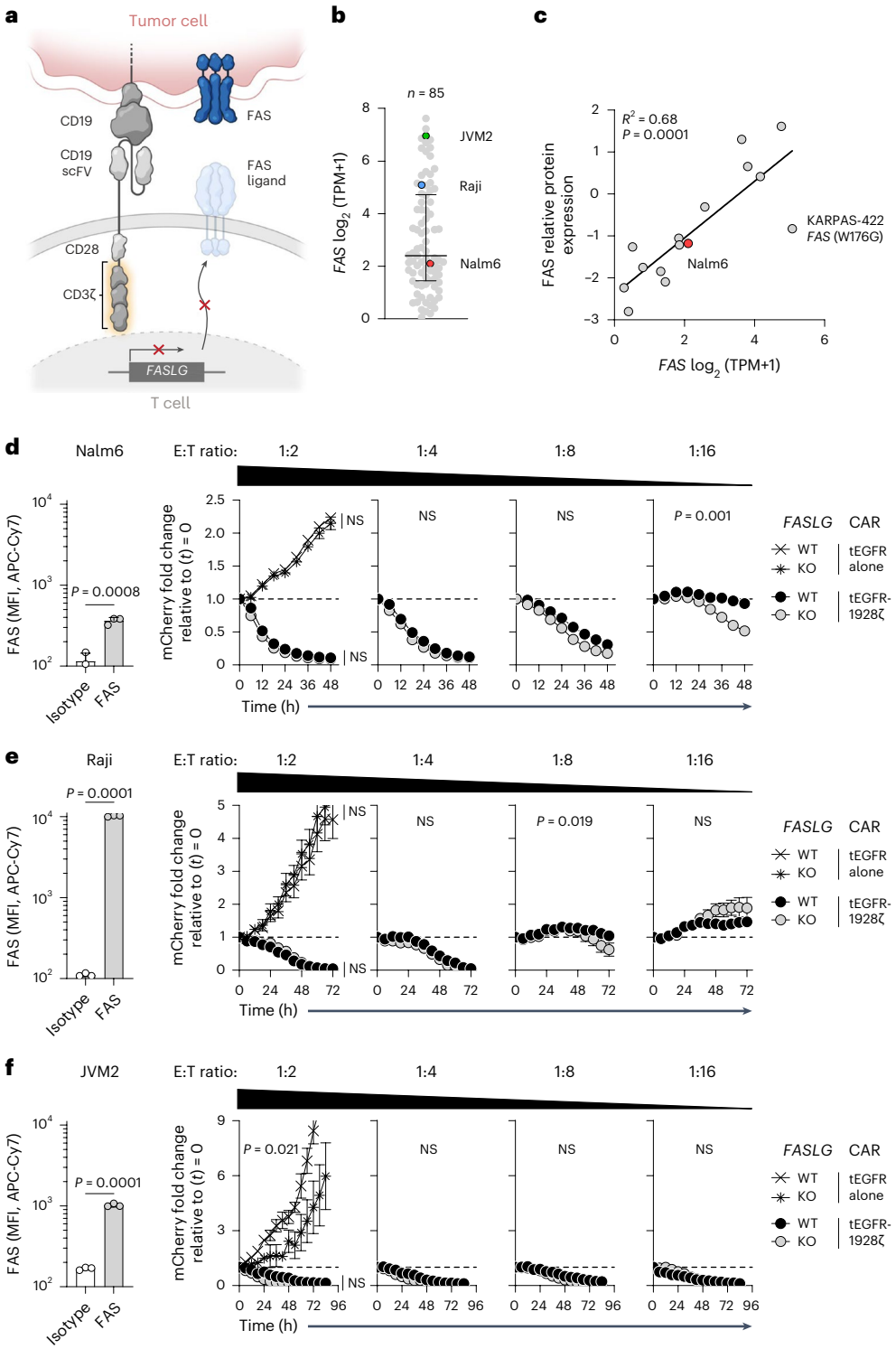

Fig. 5 | Knockout of *FASLG* in 1928ζ CAR-T cells does not impair antitumor cytolytic activity across multiple B cell cancers. a, Schematic for the CRISPR/Cas9-mediated KO of *FASLG* in human CD8$^+$ T cells expressing a 1928ζ CAR. **b**, Scatter-plot of *FAS* RNA-seq values from $n = 85$ B cell cancer lines featured in the CCLE. Horizontal line represents the median and vertical bars represent the interquartile range. TPM, transcript per million. **c**, Correlation of *FAS* transcript counts to total FAS protein levels from $n = 15$ B cell malignancy lines featured in the CCLE with matched RNA-seq and quantitative proteomic data. All cell lines express WT *FAS* except for KARPAS-422, which contains a *FAS* (W176G) mutation located in the protein's transmembrane domain. Line represents linear regression. **d**, Measurement of FAS expression on Nalm6 B-ALL cells using FACS and cytolytic activity of *FASLG* KO versus *AAVS1* KO T cells transduced with tEGFR or tEGFR-1928ζ against Nalm6/NLS–mCherry cells. **e**, Same as **d** but using Raji B-NHL and Raji/NLS–mCherry B-NHL cells. **f**, Same as in **d** but using JVM2 B cell prolymphocytic leukemia (B-PLL) and JVM2/NLS–mCherry B-PLL cells. FAS mean fluorescence intensity (MFI) values compared to an isotype control using an unpaired Student's *t*-test using $n = 3$ biologically independent samples (**d**–**f**). Cytolytic activity was measured at indicated E:T ratios using Incucyte with data shown as mean ± s.d. using $n = 3$ biologically independent samples (**d**–**f**). Statistical comparisons were performed using a one-way ANOVA. NS, not significant ($P > 0.05$). The measured *FASLG* insertion/deletion frequency following *FASLG* KO was 93.0 ± 1.0% and 95.7 ± 1.5% in T cells transduced with tEGFR alone and tEGFR-1928ζ, respectively.

https://doi.org/10.1038/s43018-025-01009-x

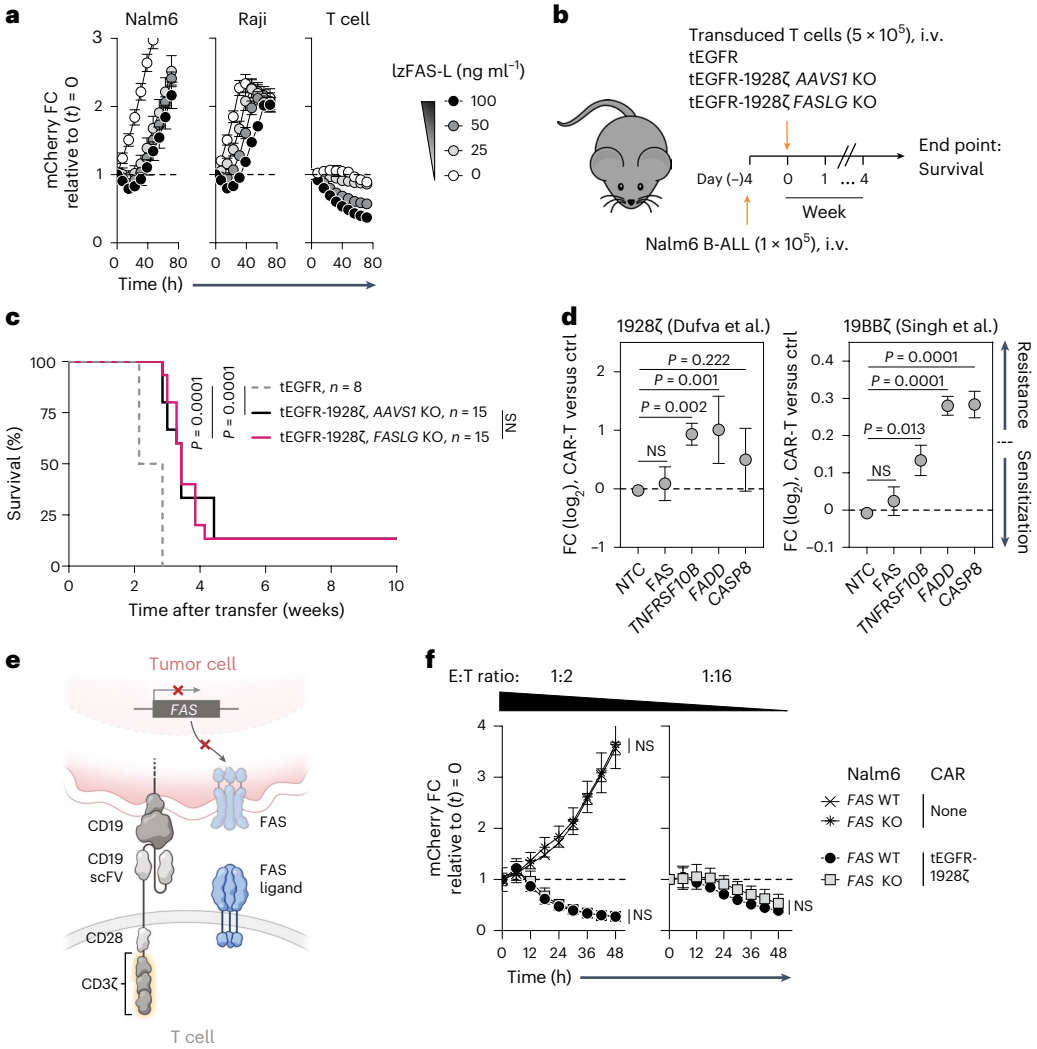

Fig. 6 | FAS-L/FAS signaling is dispensable for CAR-T antitumor efficacy. **a**, Growth kinetics of Nalm6 B-ALL, Raji B-NHL or activated T cells in the presence or absence of lzFAS-L. Each cell type was transduced with mCherry. Data are shown as mean ± s.e.m. using $n = 3$ biologically independent samples. FC, fold change. **b**,**c**, Experimental design (**b**) and Kaplan–Meier survival curve (**c**) comparing the in vivo antitumor efficacy of human $CD8^+$ T cells that express a 1928ζ CAR with CRISPR/Cas9-mediated KO of *FASLG* or *AAVS1* against established Nalm6 B-ALL. tEGFR alone, $n = 8$; tEGFR-1928ζ *AAVS1* KO, $n = 15$; tEGFR-1928ζ *FASLG* KO, $n = 15$. Statistical comparisons were made using a log-rank test. **d**, Scatter-plots displaying the enrichment or depletion of sgRNAs targeting indicated genes in the death receptor pathway by Cas9-expressing Nalm6 B-ALL cells. Tumor cells were placed under selection by T cells transduced with a 1928ζ CAR (left), a 41BBζ CAR (right) or left nontransduced as specificity controls (Ctrl). Data were reanalyzed from two published genome-scale CRISPR/Cas9 screens and are shown as mean $\log_2$FC ± s.e.m. of sgRNAs targeting indicated genes. NTC, nontargeted control sgRNAs. $n = 6$ unique sgRNAs per gene for 1928ζ CAR experiment and $n = 8$ unique sgRNAs per gene for the 19BBζ experiment. Gene level significance was determined using a one-way ANOVA corrected for multiple comparisons by Dunnett's test. **e**, Schematic for the CRISPR/Cas9-mediated KO of *FAS* using an individual sgRNA in Nalm6 B-ALL. **f**, Time-dependent cytolytic activity of 1928ζ CAR-T cells against *FAS* KO versus *FAS*-WT Nalm6/mCherry cells at a high (left) or low (right) E:T ratio. Data are shown as mean ± s.e.m. using $n = 3$ biologically independent samples. Statistical comparisons were performed using a one-way ANOVA. NS, not significant ($P > 0.05$).

transduced human T cells from two separate donors with vectors encoding tEGFR-1928ζ alone or together with ΔFAS. As an antigen-specificity control, aliquots of T cells from each donor were transduced with tEGFR alone. T cells from a single donor were adoptively transferred into mice bearing established luciferase-expressing Nalm6 tumors at a CAR-T cell dose previously determined to be noncurative (Fig. 4a)[36]. Compared to $tEGFR^+$ control T cells, we found that transfer of CAR-expressing T cells delayed tumor progression measured using bioluminescence imaging (BLI) and significantly improved overall survival (Fig. 4b–d). Mice treated with FAS signaling disrupted T cells had significantly prolonged tumor control, a finding consistent with enhanced CAR-T cell persistence.

We explored the generalizability of employing cell autonomous FAS signaling blockade to enhance the potency of CAR-T cells using a second B cell malignancy. NSG mice were pre-implanted with luciferase-expressing Raji cells, a model for aggressive B cell non-Hodgkin lymphoma (B-NHL). Tumor-bearing animals were treated with tEGFR, tEGFR-1928ζ or tEGFR-1928ζ-ΔFAS transduced T cells (Extended Data Fig. 9a–e). Similar to results in the B-ALL model, we found that ΔFAS coexpression significantly enhanced antitumor efficacy and CAR-T cell persistence. Finally, in a proof-of-concept experiment, we tested whether ΔFAS promotes the antitumor efficacy of a CAR targeting the solid tumor antigen mesothelin. Here also, ΔFAS significantly enhanced the survival of mice bearing established AsPC1 pancreatic adenocarcinoma tumors (Extended Data Fig. 9f–h). We conclude that cell-intrinsic blockade of FAS signaling enhances CAR-mediated tumor control of liquid and solid malignancies in vivo.

FAS-L is dispensable for CAR-T antitumor efficacy

We sought to define the role of *FASLG* in CAR-mediated tumor lysis. First, we compared the in vitro antitumor potency of *FASLG* KO

versus control-edited 1928ζ CAR-T cells against multiple B cell cancers (Fig. 5a). To avoid potential confounding based on differences in T cell differentiation[27,37], we enriched CD8$^+$ naive T (T_N) cells before CAR transduction. Nalm6 expresses *FAS* within the median interquartile range of B cell cancers in the Cancer Cell Line Encyclopedia and has measurable levels of total and membrane-associated FAS protein (Fig. 5b–d)[38,39]. At high E:T ratios, we observed no differences in Nalm6 lysis between *FASLG* KO and control-edited CAR-T cells (Fig. 5d). At low E:T ratios (≥1:8), however, we observed significantly greater CAR-mediated cytotoxicity by the *FASLG* KO groups. We similarly failed to measure a loss in antitumor potency using *FASLG* KO CAR-T cells against Raji and JVM2, B cell cancers with high levels of FAS (Fig. 5e,f). Without CAR-T cells, we found that a recombinant version of FAS-L oligomerized through a leucine zipper domain (lzFAS-L)[37,40] similarly had minimal impact on Nalm6 and Raji cell growth (Fig. 6a). By contrast, lzFAS-L exposure caused dose-dependent depletion of activated T cells.

We next tested whether *FASLG* was dispensable for in vivo CAR-T cell efficacy. tEGFR/1928ζ-transduced T cells underwent CRISPR/Cas9-mediated editing of *FASLG* or adeno-associated virus site 1 (*AAVS1*) as a control (Fig. 6b). Gene edited CAR-T cells or T cells transduced with tEGFR alone were transferred into Nalm6 tumor-bearing mice. Relative to tEGFR alone, both *FASLG* KO and *AAVS1* KO CAR-T cells significantly enhanced overall survival (Fig. 6c). Similar to our in vitro findings, the antitumor efficacy of *FASLG* KO CAR-T cells was not compromised.

To provide additional evidence that CAR-mediated cancer cell lysis occurs independently of the FAS-L–FAS pathway, we reanalyzed results from two published CRISPR screens[41,42]. These placed Nalm6 cells under selection by T cells expressing either a 1928ζ or 41BB (BB)-containing (19BBζ) CAR. In neither screen was enrichment for tumor clones expressing synthetic guide RNAs (sgRNAs) targeting *FAS* observed relative to nontargeted control sgRNAs (Fig. 6d). We experimentally validated this finding using a unique *FAS*-targeting sgRNA sequence (Fig. 6e,f). Unlike *FAS*, significant enrichment for sgRNAs targeting *TNFRSF10B* (the gene encoding the TRAIL-R2 death receptor) and proximal mediators of TRAIL-R2 signaling (*FADD* and *CASP8*) was observed in both screens. These findings are consistent with relatively high expression levels for *TNFRSF10B* in Nalm6 and other B cell cancer lines (Extended Data Fig. 10a,b). Correspondingly, we discovered that KO of the ligand for TRAIL-R2 (*TNFSF10*, also known as *TRAIL*) in 1928ζ CAR-T cells significantly impaired Nalm6 lysis (Extended Data Fig. 10c–e). We conclude that CAR-mediated antitumor efficacy against B cell malignancies can occur independent of the FAS-L–FAS pathway.

CAR-NK survival is regulated by a FAS-L/FAS circuit

In addition to T cells, our single-cell transcriptomic atlas revealed high levels of *FAS* and *FASLG* expression in NK cells (Fig. 1a–c). Based on this finding, we investigated whether naturally occurring and CAR-engineered NK cells express FAS protein and are sensitive to FAS-L induced apoptosis. Resting NK cells displayed minimal FAS; following activation, however, expression was significantly upregulated (Fig. 7a,b). We tested whether 1928ζ CAR-transduced NK cells and activated but nontransduced NK cells are responsive to FAS-L. Across experiments, transduction efficiencies were moderately lower for NK cells compared to T cells (Fig. 7c). Nevertheless, the efficiency of gene transfer was sufficiently high so that physical separation methods were not required for downstream analyses. Nontransduced and CAR-NK cells expressed minimal activated caspase 3/7 and annexin V, markers of early and late apoptosis (Fig. 7d). Expression of both markers significantly increased following exposure to lzFAS-L, a process that could be blocked by ΔFAS expression.

We next determined whether CAR-transduced NK cells express FAS-L protein. Lysates from NK cells transduced with tEGFR/1928ζ/ΔFAS or tLNGFR/1928ζ were probed with an anti-FAS ligand antibody by western blot. As a specificity control, an aliquot of NK cells transduced with each vector underwent CRISPR/Cas9-mediated *FASLG* editing. Similar to findings using CAR-T cells, we identified two bands with molecular weights corresponding to the membrane-bound and soluble forms of FAS-L (Fig. 7e). Both bands were nearly completely ablated following *FASLG* gene editing, confirming successful KO in NK cells. To test whether a FAS-L/FAS circuit regulates the survival of CAR-NK cells, NK cells were transduced with either tLNGFR/1928ζ or tEGFR/1928ζ/ΔFAS. tLNGFR and tEGFR-expressing CAR-NK cells were recombined 1:1 and the mixed populations were serially restimulated with CD19$^+$K562 *FASLG* KO cells or left unstimulated as controls. Following each round of tumor restimulation, we measured progressive accumulation of ΔFAS-expressing CAR-NK cells (Fig. 7f, left). Population skewing was FAS-L dependent as *FASLG* KO caused the ratio of tEGFR/tLNGFR CAR-NK cells to remain close to one. In the absence of restimulation, the proportion of each CAR-NK population remained stable indicating that *FASLG*-induced fratricide was activation dependent (Fig. 7f, right).

Naturally occurring NK cells can eliminate pathogen-infected and cancer cells through multiple mechanisms, including exocytosis of preformed cytotoxic granules and death receptor engagement[43]. To test whether CAR-NK mediated killing of a B-lymphoid malignancy is FAS-L dependent, we compared the cytolytic efficiency of CAR-transduced NK cells with or without *FASLG* KO. To distinguish between innate versus CAR-dependent effector functions, we measured killing against Raji B-NHL across a range of E:T ratios. Similar to results using CAR-T cells, we found that *FASLG* was also dispensable for CAR-NK cytotoxicity (Fig. 7g).

Finally, we sought to measure whether cell-intrinsic disruption of FAS signaling enhances the persistence of CAR-NK cells within tumor-bearing hosts. ΔFAS/tEGFR and tLNGFR/CAR-NK cells were recombined 1:1 and the mixed population co-infused into Raji tumor-bearing mice (Fig. 7h). Beginning the day of NK cell transfer, an extended half-life variant of interleukin (IL)-15 was administered by intraperitoneal (i.p.) injection to model the physiologic effect of lymphodepletion[44]. The ratio of the two engineered NK cell populations was measured in the infusion product and serially over time. We found that CAR-NK cells that coexpress ΔFAS had significantly enhanced persistence relative to CAR-NK cells alone, resulting in progressive skewing in the tEGFR/tLNGFR ratio (Fig. 7i). We conclude that a FAS-L/FAS autoregulatory circuit controls the persistence of CAR-NK cells.

ΔFAS enhances ITAM-calibrated CAR-NK cell efficacy

Similar to T cells, NK cells use adaptor proteins containing immunoreceptor tyrosine-based activation motifs (ITAMs) to drive downstream signaling[45]. Recently, we reported that an ITAM-calibrated 1928ζ CAR (henceforth 1XX CAR) enables superior T cell persistence and antitumor efficacy compared to a conventional 1928ζ CAR[46]. Whether the 1XX 1928ζ CAR also provides for superior antitumor functions when expressed by NK cells has previously not been tested. We transduced NK cells with either the native or 1XX variants of the 1928ζ CAR and measured time-dependent Raji B-NHL cytolysis (Fig. 8a). Although both groups of CAR-NK cells performed similarly at high E:T ratios, NK cells, which expressed the 1XX CAR were superior at low E:T ratios.

Based on this finding, we incorporated ΔFAS into a multi-cistronic vector encoding the 1XX CAR. We compared the antitumor efficacy of 1XX CAR-NK cells that either express or do not express ΔFAS in mice bearing established Raji B-NHL at both high and low E:T ratios. To control for potential intrinsic antitumor activity of NK cells, cohorts of mice received NK cells transduced with tEGFR alone. At a high E:T ratio, mice receiving 1XX CAR-NK cells with or without ΔFAS coexpression significantly extended animal survival compared to NK cells transduced with tEGFR alone (Fig. 8b). By contrast, when cells were administered at a low E:T ratio, we found that ΔFAS-expressing CAR-NK cells significantly prolonged survival compared to CAR-NK cells alone (Fig. 8c). We conclude that ΔFAS can enhance the in vivo antitumor potency of CAR-modified NK cells.

https://doi.org/10.1038/s43018-025-01009-x

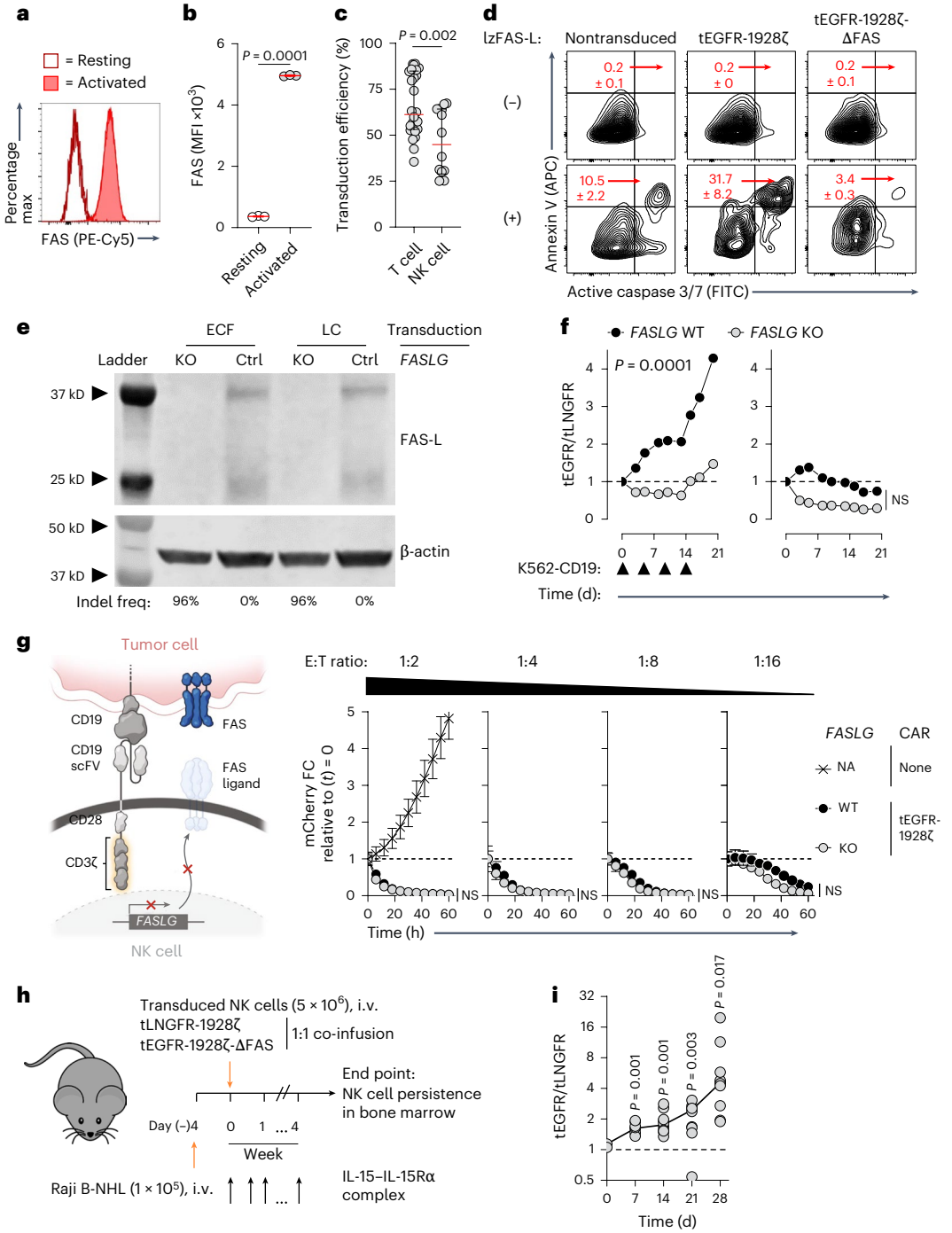

Fig. 7 | CAR-NK survival is regulated by a FAS/FAS-ligand autoregulatory circuit. a,**b**, Representative FACS (**a**) and summary scatter-plot (**b**) quantifying FAS expression by NK cells at rest and 5 d following activation. Data are shown as mean ± s.e.m. for $n = 3$ biologically independent samples. Statistical analysis was performed by two-sided Student's *t*-test. **c**, Transduction efficiencies of T cells or NK cells displayed as median ± interquartile range from $n = 26$ T cell and $n = 14$ NK cell experiments. *P* values were calculated using an unpaired two-tailed *t*-test with Welch's correction. **d**, Representative FACS plots quantifying lzFAS-L induced apoptosis in nontransduced NK cells or NK cells transduced with indicated vectors. Numbers indicate mean ± s.e.m. of activated caspase 3/7$^+$/annexin V$^+$ cells ($n = 3$ biologically independent samples). **e**, Western blot for FAS-L protein in lysates from *FASLG* KO or control (Ctrl) NK cells transduced with tEGFR-1928ζ-ΔFAS (ECF) or tLNGFR-1928ζ (LC). Frequency of frameshift Indels in *FASLG* are displayed beneath each lane. Representative results from two independent experiments are shown. **f**, Relative antigen-driven in vitro expansion of control and *FASLG* KO 1928ζ CAR-NK cells ± ΔFAS. CAR-NK cells were combined ~1:1 and serially restimulated at indicated time points with K562-CD19 *FASLG* KO cells or left unstimulated as controls. Data are displayed as the mean ratio of tEGFR$^+$/tLNGFR$^+$ cells ± s.e.m. ($n = 3$ biologically independent samples). Groups compared using a paired two-tailed Student's *t*-test for accumulated differences between each time point. NS, not significant ($P > 0.05$). **g**, Cytolysis of Raji/mCherry cells co-cultured at indicated E:T ratios with *FASLG* KO versus *FASLG*-WT tEGFR-1928ζ CAR-NK cells. Data are shown as mean ± s.e.m. ($n = 3$ biologically independent samples). Statistical comparisons were performed using a one-way ANOVA. NS, not significant ($P > 0.05$). NA, not applicable. **h**, Experimental design to test the in vivo persistence of NK cells that express a 1928ζ CAR ± ΔFAS in Raji B-NHL-bearing mice. **i**, Scatter-plot comparing the ratio of tEGFR$^+$/tLNGFR$^+$ CAR-NK cells before infusion and following adoptive transfer in the bone marrow. Symbols represent individually evaluated mice, $n = 3$ for baseline measurement and $n = 10$ per time point. *P* values compare infusion product to each time point using an unpaired, two-sided, Welch's *t*-test.

https://doi.org/10.1038/s43018-025-01009-x

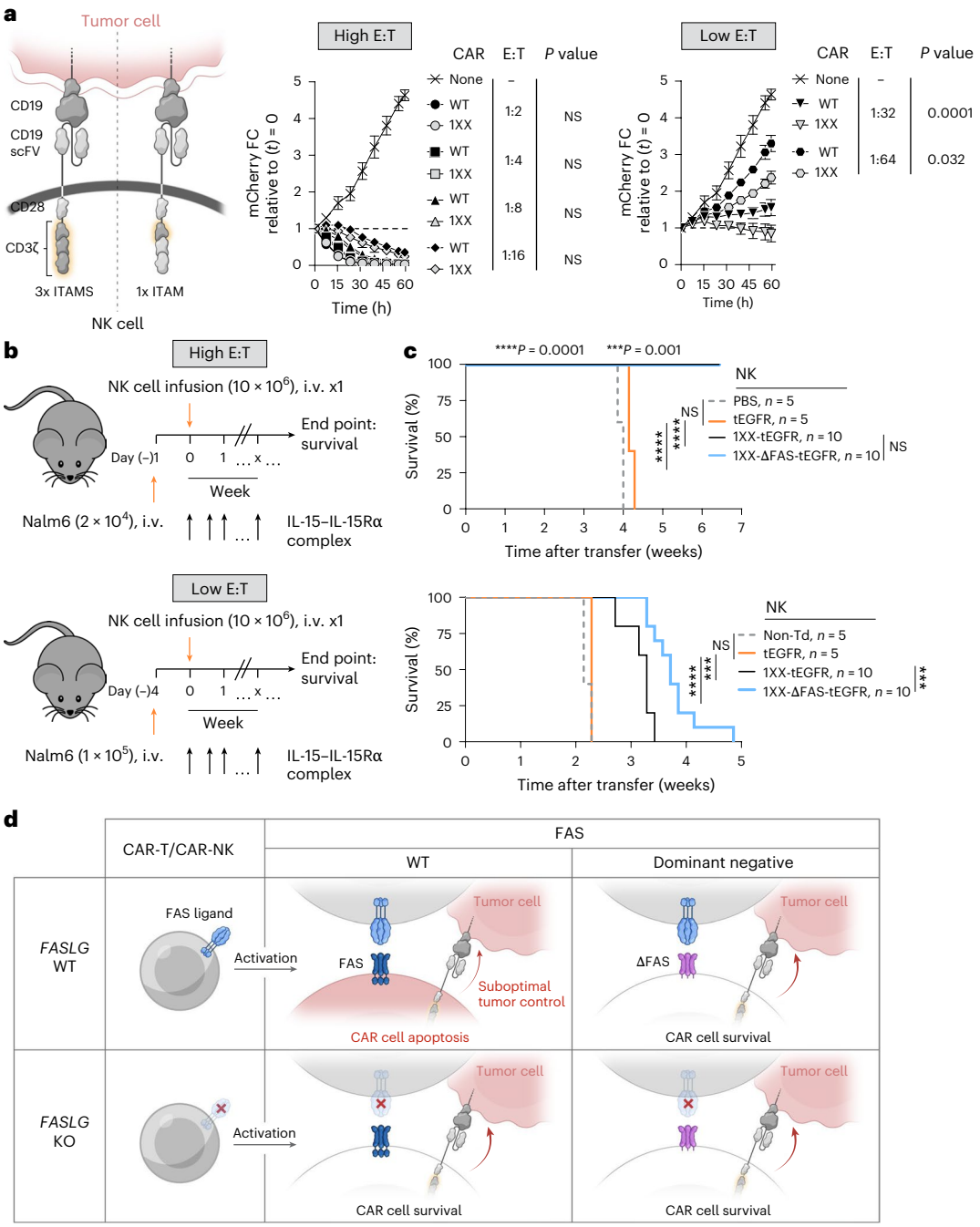

Fig. 8 | Disabling FAS signaling enhances CAR-NK antitumor efficacy in vivo. **a**, Comparison of the in vitro cytolytic efficiencies of NK cells transduced with a WT or 1XX version of the 1928ζ CAR against Nalm6/mCherry at high versus low E:T ratios. Data are shown as mean ± s.e.m. using $n = 3$ biologically independent samples. Statistical comparisons were performed using a one-way ANOVA. NS, not significant ($P > 0.05$). **b**, Experimental design to compare the in vivo antitumor efficacy of human NK cells expressing the 1XX 1928ζ CAR ± a FAS-dominant negative receptor (ΔFAS) against established Nalm6 B-ALL at a high (top) versus low (bottom) E:T ratio. All mice received a twice-weekly i.p. injection of 1 µg of IL-15 pre-complexed with IL-15Rα-Fc (1:1 M). **c**, Survival curves for high (top) versus low (bottom) E:T ratios (PBS, $n = 5$; nontransduced NK cells, $n = 5$; tEGFR alone, $n = 5$; 1XX 1928ζ-tEGFR, $n = 10$; 1XX 1928ζ-ΔFAS-tEGFR, $n = 10$). Data are plotted as Kaplan–Meier curves with groups compared using a log-rank test. NS, not significant ($P > 0.05$). **d**, Model for the dichotomous functions of FAS-L on CAR-T and CAR-NK cellular persistence and antitumor efficacy. Cells colored in red indicate FAS-L-induced apoptosis.

Discussion

Herein, we demonstrate that FAS-L performs dichotomous functions in the context of CAR-T and CAR-NK therapies targeting B cell malignancies (Fig. 8d). Whereas FAS-L limits CAR-modified lymphocyte persistence, it is expendable for CAR-mediated tumor lysis. Through analysis of a single-cell transcriptomic atlas consisting of diverse cancer types and samples from patients who received CAR-T cells, we revealed that *FASLG* expression is highly restricted. Rather than being expressed preferentially by malignant and stromal cells, as previously postulated[47,48], we found that the dominant source of *FASLG* is endogenous T cells, NK cells and CAR-modified lymphocytes. Relative to endogenous T cells, CAR-T cells displayed higher levels of *FASLG*, a finding attributable to recent encounters with antigen-bearing target cells. We further demonstrate that cellular activation promotes protein level expression of FAS-L in both CAR-T and CAR-NK cells.

Disabling FAS signaling provides a fitness advantage to CAR-expressing lymphocytes in multiple contexts. This includes following serial antigen encounter, in competitive repopulation assays in vivo, in the setting of tonic CAR-signaling, and under selection pressure by allogeneic T cells. These findings complement previous studies that found CAR designs that drive potent in vitro effector functions can lead to FAS-dependent T cell death and reduced persistence in vivo[49]. We discovered that the benefit of disrupting FAS extends beyond CAR-T to include CAR-NK cells, a lymphocyte population with favorable graft-versus-host disease risk and cytokine release profiles but relatively low engraftment potential[17]. Augmented persistence resulting from cell-intrinsic blockade of FAS signaling led to enhanced antitumor efficacy in multiple B cell tumor models and a model of pancreatic cancer. Genetic ablation of *FASLG* in CAR-modified cells removed the benefit of FAS antagonism on cell survival. Thus, CAR-modified lymphocyte persistence is negatively self-regulated through FAS-L/FAS interaction.

Unlike CAR-engineered lymphocyte survival, we established that on-target control of $CD19^+$ tumors by CAR-T and CAR-NK cells can occur independently of *FASLG*. We further demonstrated that while B-ALL and B-NHL are largely insensitive to recombinant FAS-L, T and NK cells rapidly undergo apoptosis when exposed to the ligand. These findings parallel previous studies which reported that many leukemias and lymphomas are resistant to FAS crosslinking antibodies[50,51] and that a FAS-L blocking antibody does not impair CAR-mediated cytotoxicity against B cell malignancies[52]. Correspondingly, we discovered that FAS target cell expression is dispensable for the antitumor activity of a 1928ζ CAR. Mutations in *FAS* are observed in ~5–20% of B cell malignancies[53,54]; however, these mutations frequently are subclonal[53], suggesting that they do not function as an escape mechanism from attack by endogenous immune cells. In the context of CAR-T cells, two recent studies performed next-generation sequencing on B-NHL tumor DNA before and after cell infusion to identify tumor-intrinsic resistance mechanisms. In one study, *FAS* mutations were not associated with treatment outcomes[55]. In a second study, circulating tumor DNA was analyzed before CAR-T cell infusion and at the time of disease progression[56]. Here also, mutations in *FAS* did not emerge under CAR-T cell selection in vivo. It is noteworthy that these findings do not exclude the possibility of FAS-dependent bystander killing by CAR-T cells, a phenomenon which may limit antigen-negative tumor escape[57,58]. Similarly, they do not preclude that CAR-mediated elimination of solid tumors may require FAS-L/FAS interactions, especially when other effector pathways are disrupted[52].

Beyond FAS, four additional death receptors share dependency on the FADD adaptor protein, including TNF-R1, DR3, TRAIL-R1 and TRAIL-R2 (ref. 23). *FADD* was identified as the gene most significantly associated with tumor resistance under selection by anti-CD19 CARs in two genome-scale CRISPR screens[41,42]. Both screens discovered that KO of *TNFSR10B*, the gene encoding TRAIL-R2, drove CAR-T resistance whereas *FAS* KO had no significant impact. Consistent with these findings, we found that most B cell cancer lines featured in the Cancer Cell Line Encyclopedia (CCLE) express *TNFSR10B* transcripts. Further, we identified that *TRAIL* KO significantly abrogated the antitumor efficacy of anti-CD19 CAR-T cells, a finding corroborated by other investigators[41]. Together, these data support the conclusion that death receptor signaling is an important determinant of CAR-mediated control of B cell malignancies even if FAS-L/FAS interactions are nonessential. A limitation of our study is that it focused primarily on B-ALL and B-NHL cancers. Establishing whether FAS signaling is dispensable in other malignancies, particularly a broader range of solid cancers, remains an important area of future research.

In conclusion, our findings demonstrate that disruption of FAS signaling is a broadly applicable strategy to enhance the persistence of genetically redirected lymphocytes. Based on the observation that *FASLG* expression is restricted primarily to immune cells and not cancer or stromal cells, this approach should have utility across cancer types. While our studies focused on T and NK cells, a similar strategy may benefit therapies employing invariant NK-T and γδ T cells as these lymphocyte subsets also express FAS[59,60]. Although we employed a dominant negative receptor, cell-intrinsic FAS antagonism can be accomplished using alternative methods. These include synthetic switch receptors[20,21,25,26], inhibitory RNAs[27] and CRISPR-based genome editing[18,19]. Clinical trials (NCT05617755, NCT06105021, and NCT06245915) testing several of these strategies have recently been initiated and will provide additional evidence for whether FAS-L limits cellular persistence in humans.

Methods

Ethical approvals

Our research complies with all relevant ethical guidelines. Details of the committees and institutions that approved the study protocol can be found in each specific section.

Patient materials

Bone marrow aspirate samples were obtained from patients with B-ALL who received autologous 1928ζ CAR-T cells on a Memorial Sloan Kettering Cancer Center (MSKCC) Institutional Review Board-approved protocol no. 09-114 (NCT01044069)[11]. Patients included in the analysis all had relapsed B cell ALL and were 27–77 years old (two male and one female). All patients signed an informed consent to collect biological specimens for research purposes. Participation was voluntary and no compensation was provided. Sex-specific assays were not performed. Bone marrow aspirates were collected in EDTA and bone marrow mononuclear cells (BMMCs) were isolated on the day of procurement. Aspirates were centrifuged at 800*g* for 20 min followed by aspiration of supernatant to a volume of 6 ml. Cells were resuspended in 4 ml of 2% of human serum antibody (HSA) PBS and the suspension was centrifuged again using the same settings. The buffy coat was extracted and washed once with 2% HSA PBS, and then once with 10 ml X-Vivo (Lonza). Finally, the BMMC pellet was resuspended in 1 ml of 10% dimethylsulfoxide (DMSO) in HSA cryopreservation medium and stored at −80 °C until transfer to liquid nitrogen.

RNA-FISH staining and confocal imaging

Samples procured during the conduct of NCT01044069 that satisfied the following criteria were used for analysis: (1) BMMCs were obtained within 6 weeks of CAR-T infusion; (2) the vial contained $\geq 0.5 \times 10^6$ viable mononuclear cells at the time of cryopreservation; and (3) ≥2 samples were available to avoid sample depletion. Cell pellets were placed on Superfrost Plus microscope slides (Thermo Scientific), air dried for 20 min, fixed in 4% paraformaldehyde for 15 min and then washed three times. Slides were dehydrated before being loaded into Leica Bond RX. Sections were pre-treated with EDTA-based epitope retrieval ER2 solution (Leica) for 5 min at 95 °C. Probes were hybridized for 2 h at 42 °C. The hybridized probes were detected using an RNAscope LS Multiplex Reagent kit (ACD Bio) according to the manufacturer's instructions. Tyramide conjugates were incubated with samples for 20 min at room temperature for fluorescence detection. After staining, slides were washed in PBS and incubated in 4,6-diamidino-2-phenylindole (DAPI) (Sigma Aldrich) in PBS for 5 min. PBS was rinsed and slides were mounted in Mowiol 4-88 (Calbiochem). Slides were scanned and stored at −20 °C before confocal imaging. Probes and dyes are listed in Supplementary Table 1. Slides were annotated on QuPath and gated for DAPI, scFv of 1928ζ and presence or absence of *CD3E* positivity. The fluorescence intensity of CF 488 (*FASLG*) within the nucleus (DAPI) was measured for each cell and represented as arbitrary units. This value was averaged over all cells meeting the gated expression criteria for each annotated region. For three-dimensional image reconstructions, cells were imaged using the Zeiss LSM 880 confocal microscope and Imaris imaging software.

Cell lines and tissue culture

The 293T (ATCC, CRL-3216), 293GP (Takara Bio, 631458), Nalm6 (ATCC, CRL-3273), JVM2 (ATCC, CRL-3002), Raji (ATCC, CCL-86), CFPAC-1 (ATCC, CRL-1918), NCI-H441 (ATCC, CRM-HTB-174), SW-403 (ATCC, CCL-230), CL-40 (DSMZ, ACC 535), EFM-19 (DSMZ, ACC 231), HuCCT-1 (Cytion, 300469) and SNU-1105 (KCLB, 01105) were purchased from commercial vendors. Nalm6-GFP/Luc[36] and PC3-PSMA[61] were both obtained from the Sadelain laboratory (MSKCC). Raji-GFP/Luc[62] was obtained from the Brentjens laboratory (MSKCC). K562-CD19 (ref. 63) cells were provided under a materials transfer agreement (MTA) from the Feldman laboratory (National Institutes of Health; NIH). K562 Clone 9 (ref. 64) was provided under an MTA from the Lee laboratory (Nationwide Children's Hospital). AsPC1-Luc[65] was provided by the Daniyan laboratory (MSKCC). COS-7 cells were provided under an MTA from S. A. Rosenberg (National Cancer Institute). The J8Zb2m$^-\alpha^-\beta^-$ NFAT reporter cell line was engineered and verified by our laboratory[66]. Raji and Nalm6 with stable nuclear localization sequence (NLS)–mCherry or NLS–GFP reporter expression were developed by retroviral transduction. K562-CD19 *FASLG* KO were generated by CRISPR gene editing, described below, followed by single-cell cloning. All tumor cell lines were confirmed by our laboratory and cultured in RPMI 1640 (Gibco) with 0.5% v/v pen–strep (Gibco), 1% v/v HEPES (Gibco), 0.02% v/v gentamycin (MP Biomedicals) and 10% v/v heat-inactivated fetal bovine serum (GeminiBio).

Plasmids design, viral packaging and transduction

The 1928ζ and 1XX 1928ζ sequences were provided by the Sadelain laboratory (MSKCC)[36,46]. 1928ζ, tEGFR, ΔFAS, NLS–mCherry and NLS–GFP sequences were synthesized by Genscript. The anti-CD19 scFv sequence was substituted by either an anti-PSMA[67] or anti-MSLN[65] scFv sequence to make (PSMA)28ζ and (MSLN)28ζ CARs, respectively. The HLA-A*03:01-restricted influenza and *PIK3CA* (H1047L) TCR sequences were previously described[44]. Synthesized genes were subcloned into an SFG[68] retroviral vector and the identity of the sequences was confirmed by Sanger sequencing (Genscript). For viral packaging, 293GP cells were co-transfected with pSFG and RD114 provided under MTA from the Rosenberg laboratory (NIH). Supernatant was collected on day 2 post transfection and used fresh. T cells were activated for 2 days and NK cells were activated for 4 days followed by retronectin (Takara)-mediated viral transduction. Transduction was confirmed by FACS on day 2 (for T cells and cell lines) or day 5 (for NK cells). The E:T ratio used for both in vitro and in vivo experiments was calculated based on transduction rates determined using tEGFR$^+$ or LNGFR$^+$ lymphocytes, as assessed by FACS.

Primary cell preparation

For T cell preparations, buffy coats were obtained from the New York Blood Center and STEMCELL Technologies from healthy volunteer donors after written informed consent was obtained using Institutional Review Board-approved consent forms. T cells, naive T cells and naive CD8$^+$ T cells were isolated by EasySep Human T Cell Isolation kits, EasySep Human Naive Pan T Cell Isolation kits and an EasySep Human Naive CD8$^+$ T Cell Isolation kit, respectively (STEMCELL Technologies). T cells were activated either by CD3/CD28 Dynabeads (Thermo Fisher) or ImmunoCult (STEMCELL Technologies). NK cells were isolated from cord blood mononuclear cells (STEMCELL Technologies) by EasySep Human NK Cell Isolation kits (STEMCELL Technologies) and activated by 100 Gy irradiated K562 Clone 9 feeder cells. Primary cells were cultured in RPMI 1640 (Gibco) with 1% v/v pen–strep (Gibco), 2.5% v/v HEPES (Gibco), 0.02% v/v gentamycin (MP Biomedicals) and 10% v/v heat-inactivated human serum AB (GeminiBio). Recombinant human IL-2 (PeproTech) was added to T cell and NK cell cultures at 50 IU ml^{-1} or 200 IU ml^{-1}, respectively.

Cloning and testing of an anti-HLA-A*03 TCR

Mature dendritic cells were generated from the leukapheresis product of an HLA-A*03-negative healthy donor and transfected with mRNA encoding full-length HLA-A*03:01 using the Neon transfection system. Naive CD8$^+$ T cells isolated from the same donor were stimulated with the electroporated dendritic cells at an E:T ratio of 3:1 in the presence of IL-21 (30 ng ml^{-1}), IL-7 and IL-15 (10 ng ml^{-1} each) in 24-well non-TC plates. The TCR gene sequence of the HLA-A03-binding clonotype was identified by single-cell (V)(D)(J) sequencing using the 10x Genomics platform. HLA-A*03 recognition was confirmed by retroviral TCR transduction of polyclonal T cells followed by co-culture with HLA-A*03$^+$ target cells.

Flow cytometry

For surface staining, cells were washed with PBS and stained with antibodies at 4 °C for 30 min in PBS supplemented with 0.5% FBS. Cells were washed twice with PBS + 0.5% FBS and acquired on an LSRFortessa X-20 (BD). LIVE/DEAD Fixable Aqua Dead Cell Stain kit (Thermo Fisher) was used for live-cell gating in all flow cytometry experiments. For NK cells, T cell FAS-L staining, mouse blood and tissue explants, Fc receptor blocking antibody or Human TrueStain FcX blocking solution (BioLegend) was added to cells for 10 min before staining. For intracellular staining, cells were mixed with tumor cells for 6 h in the presence of GolgiPlug (BD). As a positive control, eBioscience Cell Stimulation Cocktail (500×) (Thermo Fisher) (PMA/I) was added during the same incubation. After surface staining, cells were permeabilized and fixed by Fixation/Permeabilization kit (BD) for 20 min at 4 °C. Cells were washed once in Perm/Wash buffer (BD) and stained by antibodies for 40 min at 4 °C. Cells were washed twice with Perm/Wash buffer before acquisition. Antibody information is listed in Supplementary Table 2. The gating strategies applied to each panel for flow cytometry analysis are described in Supplementary Figs. 1 and 2.

Apoptosis assay

Flag tagged lzFAS-L was made from transfected 293T cells and enriched by Flag-conjugated beads[40]. Cells were treated with lzFAS-L at designated time points. For active caspase 3/7 staining, CellEvent Caspase 3/7 Green Detection Reagent (Thermo Fisher) was added to cultures at 20 μM and incubated for 30 min at 37 °C. Cells were washed twice with Annexin V Binding Buffer (BioLegend) and stained with APC Annexin V (BioLegend) at 5% v/v in the presence of antibodies for other surface markers. Cells were washed twice with Annexin V Binding Buffer before acquisition by FACS.

CRISPR gene editing

sgRNA (Synthego, 50 μM) and NLS-Cas9 protein (Synthego, 20 μM) were mixed at a 2.5:1 molar ratio. Cells were resuspended with P3 buffer (Lonza) for primary cells and SF buffer (Lonza) for Nalm6 cells and K562 cells. Cells were electroporated on a Lonza 4D-Nucleofector using the vendor's recommended settings for each cell type. Cells were electroporated on a Lonza 4D-Nucleofector with X Unit using vendor's recommended settings for each cell type. Cells were transferred to flasks with warmed medium immediately after electroporation. To verify gene editing, DNA was extracted from CRISPR edited cells using DNeasy Blood & Tissue kit (QIAGEN). DNA samples were PCR amplified using KOD Hot Start DNA Polymerase (Millipore Sigma) with the primers listed in Supplementary Table 3 and the PCR product was subjected to Sanger sequencing. Indel frequencies were quantified using the ICE CRISPR Analysis Tool (Synthego).

Western blot

Cells were lysed by RIPA buffer (Thermo Fisher). Lysates were shaken on a rocker and sonicated in ice water. Lysates were treated with protease inhibitors and loaded on Mini-PROTEAN TGX gel (Bio-Rad). Precision Plus Protein (Bio-Rad) was loaded as molecular weight standard. Gel was transferred to a PVDF membrane using Transblot Turbo system (Bio-Rad). The membrane was rocked and stained by primary antibody overnight at 4 °C, then rocked and stained by secondary antibody for 1 h. Antibodies used in these experiments are listed in Supplementary Table 4.

In vitro lymphocyte co-culture restimulation assays

CD19 tumor models: 1×10^6 tLNGFR-1928ζ and 1×10^6 tEGFR-1928ζ-ΔFAS-expressing cells were mixed at 1:1 ratio on day 0. For CAR-T cells, 1×10^6 K562-CD19 *FASLG* KO cells or wild-type (WT) Nalm6 cells were added to co-culture on day 0, 9 and 14. Cells were stained for flow cytometry on day 0, 2, 7, 9, 12, 14 and 17. For CAR-NK cells, 1×10^6 K562 Clone 9 *FASLG* KO tumor cells were added to co-culture on day 0, 5, 10 and 15. Cells were stained for flow cytometry on designated time points. Solid tumor models: PC3-PSMA or AsPC1 cells were used for restimulation of anti-PSMA and anti-MSLN CAR-T cells, respectively. The E:T ratio was set as 1:1 for all stimulation time points. The cell culture medium with fresh IL-2 was changed every 2–3 d during the experiments. The media volumes were measured and changed with fresh medium at the same volumes.

Xenoreactivity assays

Murine bone marrow cells and splenocytes were collected from NSG mice. Human T cells transduced with tEGFR alone or tEGFR-1928ζ were co-cultured with murine cells at a 1:1 ratio. tEGFR or tEGFR-1928ζ T cells were either co-cultured with Nalm6 cells or plated alone as controls. After 24 h, $EGFR^+$ cells were isolated by labeling with a PE-conjugated anti-EGFR antibody (BioLegend) followed by separation using an EasySep Human PE Positive Selection kit II (STEMCELL Technologies). Total RNA was isolated using an RNeasy Plus Mini kit (QIAGEN). After RNA normalization, complementary DNA was synthesized using a high-capacity cDNA Reverse Transcription kit (Applied Biosystems). TaqMan primers and probes for *GAPDH* (Hs03929097_g1) and *FASLG* (Hs00181226_g1) (Thermo Fisher) were used in mixture with cDNA and TaqMan Fast Advanced Master Mix (Applied Biosystems). Expression of *FASLG* was normalized to *GAPDH*.

In vitro T cell-mediated allogeneic-rejection assay

$CD8^+$ T cells from an HLA-A*03$^-$ healthy donor were transduced with the HLA-A*03 allo-reactive RG4382-5 TCR. As controls, T cells from the same donor were individually transduced with an HLA-A*03:01-restricted TCR that responds either to the influenza peptide (NP) or an epitope derived from the *PIK3CA* (H1047L) hotspot mutation[44]. As target cells, T cells from an HLA-A*03:01$^+$ donor were transduced either with tEGFR-1928ζ-ΔFAS or tLNGFR-1928ζ. A ~1:1 mixture of target and effector cells was co-cultured together and the ratio of tLNGFR-expressing to tEGFR-expressing CAR-T cells was measured by FACS.

Real-time live-cell imaging assays

For tumor cell-killing assays, GFP–NLS or mCherry–NLS expressing tumor cells were loaded onto 96-well plates. Plates were left at room temperature for 20 min and transferred to the Incucyte SX1 instrument (Sartorius) for baseline images. The plate was then removed from the Incucyte and loaded with lymphocytes at designated ratios. The plate was left at room temperature for 20 min again and transferred to the Incucyte for imaging. For lzFAS-L apoptosis assays, mCherry–NLS-expressing tumor or T cells were loaded onto a 96-well plate. Cells were treated with indicated concentrations of lzFAS-L. Analysis was conducted using Incucyte Basic Analysis Software.

ACT xenograft models

All mouse experiments were performed in accordance with an MSKCC Institutional Animal Care and Use Committee-approved protocol (19-08-013). The 6–10-week-old female NOD.Cg-Prkdc^{scid} Il2rg^{tm1Wjl}/SzJ (NSG) mice were used for all animal experiments (Jackson Laboratory) and housed in pathogen-free conditions at the MSKCC vivarium. Sex was not considered in the design of mouse experiments. The mouse room maintained a 12-h light–dark cycle, temperature of 65–75 °F and humidity levels of 40–60%. Mice were randomized for all group designs. Nalm6-Luc or Raji-Luc cells were given by tail vein in 200 µl PBS. AsPC1-Luc cells were given by subcutaneous injection in 100 µl of a 1:1 mixture of Matrigel (Corning) and serum-free RPMI medium. CAR-T, CAR-NK or control cells were also administered by tail vein injection in 200 µl PBS on indicated days after tumor inoculation. For mice that received anti-MSLN CAR-T cells or NK cells, IL-15 (Peprotech)/IL-15Rα (R&D Systems) complex was administered i.p. at a final concentration of 1 µg of IL-15 per mouse twice weekly for the duration of the experiment. Tumor burden was measured by bioluminescence using IVIS Imaging System (PerkinElmer) and analyzed using the Living Image software (PerkinElmer)[46]. The complex was freshly prepared by incubating recombinant human IL-15 (Peprotech, 200-15) with IL-15Rα-Fc (R&D Systems, 7194-IR) at a 1:1 molar ratio for 30 min at 37 °C and administered at a final concentration of 1 µg of IL-15 per mouse. Health conditions of mice were monitored by MSKCC Research Animal Resource Center. The maximum tumor volume for solid tumors was set at 1,000 mm^3 with no exceptions and was not exceeded. All injections, BLI images and decisions to kill were carried out by veterinary staff blinded to the identity of the treatment groups. Killing was performed based on tumor volume limit or predetermined clinical criteria, including loss of >10% body weight, development of hind limb paralysis, hunched posture, labored breathing, scruffy coat, cage mate avoidance and lethargy.

Tissue collection and sample preparation

After killing mice with CO_2, tissues were dissected and kept in PBS with 1 mM EDTA (EMD Millipore). Tissues were processed using 100-µm cell strainers (Falcon). For retro-orbital blood collection, 100 µl of blood was collected from each mouse. Processed tissue cells and blood cells were centrifuged at 335*g* for 5 min and resuspended in ACK lysing buffer (Gibco) for 20 min at room temperature. Cells were filtered through Flowmi 70-µm cell strainers (Bel-Art). Cells were washed once with PBS supplemented with 1 mM EDTA and resuspended in FcR blocking buffer using Human TruStain FcX (BioLegend) and Mouse TruStain FcX PLUS (BioLegend) at room temperature for 15 min. To quantify peripheral blood cell absolute concentration, stained cells were resuspended in 400 µl and mixed with 20-µl CountBright beads (Thermo Fisher). Final concentrations (cells per µl) were calculated as concentration = (number of cell events/number of bead events) × (assigned bead count of the lot/volume of sample).

Bulk and single-cell RNA sequencing datasets and processing

TISCH datasets were uniformly processed with MAESTRO[69] (which included removal of low-quality cells, cell-type annotation and malignant cell identification). Only TISCH-annotated (thus filtered) cells were retained. For datasets GSE111360 and GSE176021 lacking TISCH annotations, cells were filtered out if the number of detected genes was <500, and features were removed if they were expressed in <10 cells; cell types were then annotated with SingleR (v.1.0.6)[70] with reference to the TISCH-annotated datasets. Cells from all datasets were combined and integrated with the fastMNN function from batchelor (v.1.10.0)[71] using the top 2,000 most variable genes. Dimensionality reduction was performed with runUMAP from scater (v.1.22.0)[72] on the batch-corrected values. Size-factor normalized log counts were obtained via computeSumFactors from scran (v.1.22.1)[73] and logNormCounts from scater (v.1.22.0). UMAPs and violin plots of *FAS* and *FASLG* were visualized with scater (v.1.22.0) and dittoSeq (v.1.6.0)[74]. For patients who had received 1928ζ CAR-T cell therapy, processed scRNA-seq data were downloaded from the Data Availability section of a previously published study[29]. CAR-T cells were defined as either (1) cells profiled following an anti-FMC63 sort; or (2) peripheral blood mononuclear cells where ≥1 CAR-T transcripts were detected. Data were summarized as the fraction of *FASLG*$^+$ cells requiring a minimum of one unique molecular identifier per cell. Data were split based on per-cell annotations provided in the data object shared by the authors.

Whole-genome CRISPR screen re-analysis

Count matrices from two previously published whole-genome screens[41,42] were reanalyzed using MAGeCK (v.0.5.9.2) with default parameters[75].

Statistics and reproducibility

No statistical methods were used to predetermine sample sizes. Our sample sizes are similar to those reported in previous publications[24,76,77]. Appropriate statistical tests were used to analyze data, as described in each figure legend. Data distribution was assumed to be normal, but this was not formally tested. Statistical analyses were performed with GraphPad Prism v.10 software. Significance was preset at P values < 0.05. In vitro experimental data were generated from experiments containing $n = 3$ independent cultures per condition. For in vivo mouse experiments, treatment groups had $n = 5$–15 mice per condition, and control groups had $n = 5$–10 mice as described in figures and figure legends. Cell injection, drug administration and data acquisition were performed by investigators blinded to treatment groups. No data were excluded from any analyses.

Reporting summary

Further information on research design is available in the Nature Portfolio Reporting Summary linked to this article.

Data availability

Previously published bulk RNA-seq datasets (pan-cancer, skin cutaneous melanoma, lung adenocarcinoma, breast invasive carcinoma, ovarian serous cystadenocarcinoma and pancreatic adenocarcinoma) resulting from the TCGA Research Network (https://www.cancer.gov/tcga) were reanalyzed using cBioPortal[78]. Publicly available scRNA-seq datasets from patients who had not received previous CAR-T therapy were assembled from the eight studies listed in Extended Data Fig. 2. Raw count matrices were retrieved from the Gene Expression Omnibus using accession numbers GSE132509, GSE111014, GSE117570, GSE111360, GSE148190, GSE146771, GSE176021 and GSE139829. When available, cell annotations were retrieved from TISCH[79]. Raw count matrices for publicly available scRNA-seq datasets from patients who had previous 1928ζ CAR-T therapy are available from GSE197268. Count matrices from whole-genome CRISPR/Cas9 screens are available in supplementary tables of the related publication[42] or GSE130663. The remaining data are available within the Article, Supplementary Information and Source Data file and/or from the corresponding author on request. Source data are provided with this paper.

Code availability

Code is available at https://github.com/abcwcm/Yi2024.

References

1. Cappell, K. M. & Kochenderfer, J. N. Long-term outcomes following CAR T cell therapy: what we know so far. *Nat. Rev. Clin. Oncol.* **20**, 359–371 (2023).
2. June, C. H. & Sadelain, M. Chimeric antigen receptor therapy. *N. Engl. J. Med.* **379**, 64–73 (2018).
3. Brown, C. E. et al. Regression of glioblastoma after chimeric antigen receptor T-cell therapy. *N. Engl. J. Med.* **375**, 2561–2569 (2016).
4. Hegde, M. et al. Tumor response and endogenous immune reactivity after administration of HER2 CAR T cells in a child with metastatic rhabdomyosarcoma. *Nat. Commun.* **11**, 3549 (2020).
5. Qi, C. et al. Claudin18.2-specific CAR T cells in gastrointestinal cancers: phase 1 trial interim results. *Nat. Med.* **28**, 1189–1198 (2022).
6. Majzner, R. G. et al. GD2-CAR T cell therapy for H3K27M-mutated diffuse midline gliomas. *Nature* **603**, 934–941 (2022).
7. Mackensen, A. et al. CLDN6-specific CAR-T cells plus amplifying RNA vaccine in relapsed or refractory solid tumors: the phase 1 BNT211-01 trial. *Nat. Med.* **29**, 2844–2853 (2023).
8. Heczey, A. et al. Anti-GD2 CAR-NKT cells in relapsed or refractory neuroblastoma: updated phase 1 trial interim results. *Nat. Med.* **29**, 1379–1388 (2023).
9. Del Bufalo, F. et al. GD2-CART01 for relapsed or refractory high-risk neuroblastoma. *N. Engl. J. Med.* **388**, 1284–1295 (2023).
10. Ruella, M., Korell, F., Porazzi, P. & Maus, M. V. Mechanisms of resistance to chimeric antigen receptor-T cells in haematological malignancies. *Nat. Rev. Drug Discov.* **22**, 976–995 (2023).
11. Park, J. H. et al. Long-term follow-up of CD19 CAR therapy in acute lymphoblastic leukemia. *N. Engl. J. Med.* **378**, 449–459 (2018).
12. Kochenderfer, J. N. et al. Lymphoma remissions caused by anti-CD19 chimeric antigen receptor T cells are associated with high serum interleukin-15 Levels. *J. Clin. Oncol.* https://doi.org/10.1200/jco.2016.71.3024 (2017).
13. Fraietta, J. A. et al. Determinants of response and resistance to CD19 chimeric antigen receptor (CAR) T cell therapy of chronic lymphocytic leukemia. *Nat. Med.* **24**, 563–571 (2018).
14. Wang, M. et al. KTE-X19 CAR T-cell therapy in relapsed or refractory mantle-cell lymphoma. *N. Engl. J. Med.* **382**, 1331–1342 (2020).
15. Munshi, N. C. et al. Idecabtagene vicleucel in relapsed and refractory multiple myeloma. *N. Engl. J. Med.* **384**, 705–716 (2021).
16. Marin, D. et al. Safety, efficacy and determinants of response of allogeneic CD19-specific CAR-NK cells in CD19(+) B cell tumors: a phase 1/2 trial. *Nat. Med.* https://doi.org/10.1038/s41591-023-02785-8 (2024).
17. Myers, J. A. & Miller, J. S. Exploring the NK cell platform for cancer immunotherapy. *Nat. Rev. Clin. Oncol.* **18**, 85–100 (2021).
18. Freitas, K. A. et al. Enhanced T cell effector activity by targeting the Mediator kinase module. *Science* **378**, eabn5647 (2022).
19. Menegatti, S. et al. Ablation of FAS confers allogeneic CD3(-) CAR T cells with resistance to rejection by T cells and natural killer cells. *Nat. Biomed. Eng.* https://doi.org/10.1038/s41551-024-01282-8 (2024).
20. Roth, T. L. et al. Pooled knockin targeting for genome engineering of cellular immunotherapies. *Cell* **181**, 728–744 e721 (2020).
21. Blaeschke, F. et al. Modular pooled discovery of synthetic knockin sequences to program durable cell therapies. *Cell* **186**, 4216–4234 e4233 (2023).
22. Tieu, V. et al. A versatile CRISPR-Cas13d platform for multiplexed transcriptomic regulation and metabolic engineering in primary human T cells. *Cell* https://doi.org/10.1016/j.cell.2024.01.035 (2024).
23. Yi, F., Frazzette, N., Cruz, A. C., Klebanoff, C. A. & Siegel, R. M. Beyond cell death: new functions for TNF family cytokines in autoimmunity and tumor immunotherapy. *Trends Mol. Med.* **24**, 642–653 (2018).
24. Yamamoto, T. N. et al. T cells genetically engineered to overcome death signaling enhance adoptive cancer immunotherapy. *J. Clin. Invest.* **129**, 1551–1565 (2019).
25. Oda, S. K. et al. A Fas-4-1BB fusion protein converts a death to a pro-survival signal and enhances T cell therapy. *J. Exp. Med.* **217**, e20191166 (2020).
26. McKenzie, C. et al. Novel Fas-TNFR chimeras that prevent Fas ligand-mediated kill and signal synergistically to enhance CAR T cell efficacy. *Mol. Ther. Nucleic Acids* **32**, 603–621 (2023).
27. Dotti, G. et al. Human cytotoxic T lymphocytes with reduced sensitivity to Fas-induced apoptosis. *Blood* **105**, 4677–4684 (2005).
28. James, S. E. et al. Leucine zipper-based immunomagnetic purification of CAR T cells displaying multiple receptors. *Nat. Biomed. Eng.* **8**, 1592–1614 (2024).
29. Haradhvala, N. J. et al. Distinct cellular dynamics associated with response to CAR-T therapy for refractory B cell lymphoma. *Nat. Med.* **28**, 1848–1859 (2022).
30. Wang, X. et al. A transgene-encoded cell surface polypeptide for selection, in vivo tracking, and ablation of engineered cells. *Blood* **118**, 1255–1263 (2011).

31. Gallardo, H. F., Tan, C. & Sadelain, M. The internal ribosomal entry site of the encephalomyocarditis virus enables reliable coexpression of two transgenes in human primary T lymphocytes. *Gene Ther.* **4**, 1115–1119 (1997).
32. Siegel, R. M. et al. Fas preassociation required for apoptosis signaling and dominant inhibition by pathogenic mutations. *Science* **288**, 2354–2357 (2000).
33. Szymczak, A. L. et al. Correction of multi-gene deficiency in vivo using a single 'self-cleaving' 2A peptide-based retroviral vector. *Nat. Biotechnol.* **22**, 589–594 (2004).
34. Tsuchida, C. A. et al. Mitigation of chromosome loss in clinical CRISPR-Cas9-engineered T cells. *Cell* **186**, 4567–4582 e4520 (2023).
35. Kayagaki, N. et al. Metalloproteinase-mediated release of human Fas ligand. *J. Exp. Med.* **182**, 1777–1783 (1995).
36. Brentjens, R. J. et al. Genetically targeted T cells eradicate systemic acute lymphoblastic leukemia xenografts. *Clin. Cancer Res.* **13**, 5426–5435 (2007).
37. Klebanoff, C. A. et al. Memory T cell-driven differentiation of naive cells impairs adoptive immunotherapy. *J. Clin. Invest.* **126**, 318–334 (2016).
38. Ghandi, M. et al. Next-generation characterization of the Cancer Cell Line Encyclopedia. *Nature* **569**, 503–508 (2019).
39. Nusinow, D. P. et al. Quantitative proteomics of the Cancer Cell Line Encyclopedia. *Cell* **180**, 387–402 e316 (2020).
40. Cruz, A. C. et al. Fas/CD95 prevents autoimmunity independently of lipid raft localization and efficient apoptosis induction. *Nat. Commun.* **7**, 13895 (2016).
41. Singh, N. et al. Impaired death receptor signaling in leukemia causes antigen-independent resistance by inducing CAR T-cell dysfunction. *Cancer Discov.* **10**, 552–567 (2020).
42. Dufva, O. et al. Integrated drug profiling and CRISPR screening identify essential pathways for CAR T-cell cytotoxicity. *Blood* **135**, 597–609 (2020).
43. Prager, I. et al. NK cells switch from granzyme B to death receptor-mediated cytotoxicity during serial killing. *J. Exp. Med.* **216**, 2113–2127 (2019).
44. Chandran, S. S. et al. Immunogenicity and therapeutic targeting of a public neoantigen derived from mutated PIK3CA. *Nat. Med.* **28**, 946–957 (2022).
45. Bryceson, Y. T., March, M. E., Ljunggren, H. G. & Long, E. O. Activation, coactivation, and costimulation of resting human natural killer cells. *Immunol. Rev.* **214**, 73–91 (2006).
46. Feucht, J. et al. Calibration of CAR activation potential directs alternative T cell fates and therapeutic potency. *Nat. Med.* **25**, 82–88 (2019).
47. O'Connell, J., Bennett, M. W., O'Sullivan, G. C., Collins, J. K. & Shanahan, F. Fas counter-attack–the best form of tumor defense? *Nat. Med.* **5**, 267–268 (1999).
48. Peter, M. E. et al. The role of CD95 and CD95 ligand in cancer. *Cell Death Differ.* **22**, 549–559 (2015).
49. Kunkele, A. et al. Functional tuning of CARs reveals signaling threshold above which $CD8^+$ CTL antitumor potency is attenuated due to cell Fas-FasL-dependent AICD. *Cancer Immunol. Res.* **3**, 368–379 (2015).
50. Karawajew, L. et al. Differential CD95 expression and function in T and B lineage acute lymphoblastic leukemia cells. *Leukemia* **11**, 1245–1252 (1997).
51. Plumas, J. et al. Tumor B cells from non-Hodgkin's lymphoma are resistant to CD95 (Fas/Apo-1)-mediated apoptosis. *Blood* **91**, 2875–2885 (1998).
52. Montalvo, M. J. et al. Decoding the mechanisms of chimeric antigen receptor (CAR) T cell-mediated killing of tumors: insights from granzyme and Fas inhibition. *Cell Death Dis.* **15**, 109 (2024).
53. Chapuy, B. et al. Molecular subtypes of diffuse large B cell lymphoma are associated with distinct pathogenic mechanisms and outcomes. *Nat. Med.* **24**, 679–690 (2018).
54. Landowski, T. H., Qu, N., Buyuksal, I., Painter, J. S. & Dalton, W. S. Mutations in the Fas antigen in patients with multiple myeloma. *Blood* **90**, 4266–4270 (1997).
55. Jain, M. D. et al. Whole-genome sequencing reveals complex genomic features underlying anti-CD19 CAR T-cell treatment failures in lymphoma. *Blood* **140**, 491–503 (2022).
56. Sworder, B. J. et al. Determinants of resistance to engineered T cell therapies targeting CD19 in large B cell lymphomas. *Cancer Cell* **41**, 210–225 e215 (2023).
57. Hong, L. K. et al. CD30-redirected chimeric antigen receptor T cells target CD30(+) and CD30(-) embryonal carcinoma via antigen-dependent and Fas/FasL interactions. *Cancer Immunol. Res.* **6**, 1274–1287 (2018).
58. Upadhyay, R. et al. A critical role for Fas-mediated off-target tumor killing in T-cell immunotherapy. *Cancer Discov.* **11**, 599–613 (2021).
59. Xu, X. et al. NKT cells coexpressing a GD2-specific chimeric antigen receptor and IL15 show enhanced in vivo persistence and antitumor activity against neuroblastoma. *Clin. Cancer Res.* **25**, 7126–7138 (2019).
60. Deniger, D. C. et al. Activating and propagating polyclonal γδ T cells with broad specificity for malignancies. *Clin. Cancer Res.* **20**, 5708–5719 (2014).
61. Gong, M. C. et al. Cancer patient T cells genetically targeted to prostate-specific membrane antigen specifically lyse prostate cancer cells and release cytokines in response to prostate-specific membrane antigen. *Neoplasia* **1**, 123–127 (1999).
62. Lee, J. C. et al. In vivo inhibition of human CD19-targeted effector T cells by natural T regulatory cells in a xenotransplant murine model of B cell malignancy. *Cancer Res.* **71**, 2871–2881 (2011).
63. Kochenderfer, J. N. et al. Construction and preclinical evaluation of an anti-CD19 chimeric antigen receptor. *J. Immunother.* **32**, 689–702 (2009).
64. Denman, C. J. et al. Membrane-bound IL-21 promotes sustained ex vivo proliferation of human natural killer cells. *PLoS ONE* **7**, e30264 (2012).
65. Cai, W. et al. Augmenting CAR T-cell Functions with LIGHT. *Cancer Immunol. Res.* **12**, 1361–1379 (2024).
66. Notti, R. Q. et al. The resting and ligand-bound states of the membrane-embedded human T-cell receptor-CD3 complex. Preprint at *bioRxiv* https://doi.org/10.1101/2023.08.22.554360 (2024).
67. Liu, H. et al. Monoclonal antibodies to the extracellular domain of prostate-specific membrane antigen also react with tumor vascular endothelium. *Cancer Res.* **57**, 3629–3634 (1997).
68. Riviere, I., Brose, K. & Mulligan, R. C. Effects of retroviral vector design on expression of human adenosine deaminase in murine bone marrow transplant recipients engrafted with genetically modified cells. *Proc. Natl Acad. Sci. USA* **92**, 6733–6737 (1995).
69. Wang, C. et al. Integrative analyses of single-cell transcriptome and regulome using MAESTRO. *Genome Biol.* **21**, 198 (2020).
70. Aran, D. et al. Reference-based analysis of lung single-cell sequencing reveals a transitional profibrotic macrophage. *Nat. Immunol.* **20**, 163–172 (2019).
71. Haghverdi, L., Lun, A. T. L., Morgan, M. D. & Marioni, J. C. Batch effects in single-cell RNA-sequencing data are corrected by matching mutual nearest neighbors. *Nat. Biotechnol.* **36**, 421–427 (2018).
72. McCarthy, D. J., Campbell, K. R., Lun, A. T. & Wills, Q. F. Scater: pre-processing, quality control, normalization and visualization of single-cell RNA-seq data in R. *Bioinformatics* **33**, 1179–1186 (2017).
73. Lun, A. T., McCarthy, D. J. & Marioni, J. C. A step-by-step workflow for low-level analysis of single-cell RNA-seq data with Bioconductor. *F1000Res* **5**, 2122 (2016).

74. Bunis, D. G., Andrews, J., Fragiadakis, G. K., Burt, T. D. & Sirota, M. dittoSeq: universal user-friendly single-cell and bulk RNA sequencing visualization toolkit. *Bioinformatics* **36**, 5535–5536 (2021).
75. Li, W. et al. MAGeCK enables robust identification of essential genes from genome-scale CRISPR/Cas9 knockout screens. *Genome Biol.* **15**, 554 (2014).
76. Li, Y. et al. KIR-based inhibitory CARs overcome CAR-NK cell trogocytosis-mediated fratricide and tumor escape. *Nat. Med.* **28**, 2133–2144 (2022).
77. Sabatino, M. et al. Generation of clinical-grade CD19-specific CAR-modified CD8$^+$ memory stem cells for the treatment of human B-cell malignancies. *Blood* **128**, 519–528 (2016).
78. Cerami, E. et al. The cBio cancer genomics portal: an open platform for exploring multidimensional cancer genomics data. *Cancer Discov.* **2**, 401–404 (2012).
79. Sun, D. et al. TISCH: a comprehensive web resource enabling interactive single-cell transcriptome visualization of tumor microenvironment. *Nucleic Acids Res.* **49**, D1420–D1430 (2021).

Acknowledgements

This study was supported in part by NIH R37 CA259177, R01 CA286507, R01 CA269733 and P50 CA217694 (C.A.K.); P30 CA008748 (C.A.K., C.S.H., A.F.D., K.C.H. and C.A.L.); W. H. Goodwin and A. Goodwin and the Commonwealth Foundation for Cancer Research (C.A.K.); The Center for Experimental Therapeutics at Memorial Sloan Kettering Cancer Center (C.A.K., A.F.D. and K.S.H.); The MSK Technology Development Fund (C.A.K., C.S.H. and A.F.D.); The Parker Institute for Cancer Immunotherapy (C.A.K.); The Sarcoma Center at MSKCC (C.A.K.); The Damon Runyon Cancer Research Foundation CI-96-18 (C.A.K.); the Geoffrey Beene Cancer Research Center (C.A.K.); the Tow Center for Developmental Oncology (C.A.K., F.Y. and T.C.); Cycle for Survival (C.A.K. and A.F.D.); and the Metropoulos Family Foundation (C.A.K.). F.Y. was supported in part by an immuno-oncology research fellowship from the William Randolph Hearst Foundation and the Parker Institute for Cancer Immunotherapy. T.C. was supported in part by a Career Development Award from the Tow Center for Developmental Oncology. J.F. was supported by the Starting Grant of the European Research Council, ERC-StG-949667. M.V.G. was supported in part by a Conquer Cancer Young Investigator Award, The Damon Runyon Cancer Research Foundation and the Louis V. Gerstner, Jr Physician Scholars Program. C.S.H. was supported in part by the MSK Paul Calabresi Career Development Award for Clinical Oncology (K12 CA184746), NIH SPORE in Soft Tissue Sarcoma (P50 CA217694), Ira Schneider Memorial Cancer Research Foundation, and NIH grant 1U 01CA256801. K.N.K. was supported by the German Research Foundation, the MSKCC's Center for Experimental Immuno-Oncology and the Melanoma Research Foundation. I.E. was supported in part by the Cancer Research Institute and the Melanoma Research Foundation. A.F.D. was supported in part by NIH P50 CA254838. C.A.L. was supported in part by NIH grants R00 HG012579 and U01 AT012984. K.C.H. was supported in part by NIH grants R01 HL155741, R01 AI150999 and U01 AI1069197. The funders had no role in the study design, data collection, data analysis, decision to publish or preparation of the manuscript. The content is solely the responsibility of the authors and does not necessarily represent the official views of the NIH. Original artwork featured in Figs. 2 and 5–8 and Extended Data Fig. 10 were performed with the assistance of SciStories.

Author contributions

F.Y. and C.A.K. conceived of and designed all experiments. F.Y., T.C., N.Z., R.E., E.J.B., H.A., M.V.G., C.S.H., I.E. and S.S.C. performed or supported in vitro experiments. F.Y. and T.C. performed and analyzed RNA-FISH confocal imaging and western blot experiments. F.Y., T.C., N.Z. and R.E. generated cell products and analyzed data resulting from in vivo animal studies. F.D., P.Z., C.A.L. and D.B. assembled and analyzed scRNA-seq data using publicly available data. K.N.K. reanalyzed results from publicly available CRISPR screens. J.H.P. contributed clinically annotated patient samples. J.F., S.S.C., K.C.H., Z.Z., W.C., A.F.D. and M.S. provided key materials, reagents and technical know-how. K.C.H. and M.S. provided additional study supervision. C.A.K. and F.Y. wrote the initial and revised manuscripts with input and contributions from all authors. All authors approved the revised manuscript.

Competing interests

C.A.K. and F.Y. are inventors on patents (PCT/US2021/0214415, 'Immunoresponsive cells expressing dominant negative FAS and uses thereof' and PCT/US2023/005877, 'Novel dominant negative FAS polypeptides, cells comprising thereof and uses thereof') related to this work. J.F. and M.S. are inventors on a patent (PCT/ US18/68134, 'Enhanced chimeric antigen receptors and uses thereof') related to this work which has been licensed to Atara Biotherapeutics, Fate Therapeutics, Takeda Pharmaceuticals, Mnemo Therapeutics and Minerva Biotechnologies. C.A.K. is a scientific co-founder and holds equity in Affini-T Therapeutics. C.A.K. has previously consulted for, or is on the scientific and/or clinical advisory boards of, Achilles Therapeutics, Affini-T Therapeutics, Aleta BioTherapeutics, Bellicum Pharmaceuticals, BMS, Catamaran Bio, Cell Design Labs, Decheng Capital, G1 Therapeutics, Klus Pharma, Obsidian Therapeutics, PACT Pharma, Roche/Genentech, Royalty Pharma, Stereo Biotherapeutics and T-knife. S.S.C. is a scientific advisor and equity holder in Affini-T Therapeutics. A.F.D. is the chief scientific officer of Promicell Therapeutics and holds equity in the company. A.F.D. is listed as an inventor on multiple patents related to CAR-T cell therapy and may be eligible to receive a portion of royalties paid to MSK by Caribou Biosciences, Tigen Pharma SA, Promicell Therapeutics and other entities that have optioned or licensed these technologies from MSK. C.A.L. is a scientific co-founder and holds equity in Cartography Biosciences. J.H.P. received consulting fees from Adaptive Biotechnologies, Affyimmune Therapeutics, Amgen, Autolus, Ascentage, Be Biopharma, Beigene, Bright Pharmaceutical Services, Caribou Biosciences, Curocell, Galapagos, In8Bio, Iovance, Jazz Pharmaceuticals, Kite, Medpace, Pfizer, Servier, Sobi, Synthekine and Takeda; received honoraria from OncLive, Physician Education Resource and MJH Life Sciences; serves on scientific advisory board of Allogene Therapeutics, Artiva Biotherapeutics and Green Cross Biopharma; and received institutional research funding from Autolus, Genentech, Fate Therapeutics, InCyte, Servier and Takeda. M.S. reports grants from Atara Biotherapeutics, Fate Therapeutics, Mnemo Therapeutics and Takeda outside the submitted work. Additionally, M.S. has patents issued and licensed to Juno Therapeutics, Atara Biotherapeutics, Fate Therapeutics, Takeda Pharmaceuticals and Alaya Bio. The remaining authors declare no competing interests.

Additional information

Extended data is available for this paper at https://doi.org/10.1038/s43018-025-01009-x.

Supplementary information The online version contains supplementary material available at https://doi.org/10.1038/s43018-025-01009-x.

Correspondence and requests for materials should be addressed to Christopher A. Klebanoff.

Peer review information *Nature Cancer* thanks Joshua Brody, Saar Gill and Nathan Singh for their contribution to the peer review of this work.

[1]Immuno-Oncology Program, Memorial Sloan Kettering Cancer Center (MSKCC), New York, NY, USA. [2]Department of Pediatric Hematology/Oncology, Weill Cornell Medical College, New York, NY, USA. [3]Department of Physiology and Biophysics, Weill Cornell Medicine, New York, NY, USA. [4]Applied Bioinformatics Core, Weill Cornell Medicine, New York, NY, USA. [5]Catenion, Berlin, Germany. [6]Center for Cell Engineering, MSKCC, New York, NY, USA. [7]Cluster of Excellence iFIT, University Children's Hospital Tübingen, Tübingen, Germany. [8]Cell Therapy Service, Department of Medicine, MSKCC, New York, NY, USA. [9]Department of Medicine, Weill Cornell Medicine, New York, NY, USA. [10]Columbia Initiative in Cell Engineering and Therapy, Columbia University, New York, NY, USA. [11]Molecular Pharmacology Program, MSKCC, New York, NY, USA. [12]Leukemia Service, Department of Medicine, MSKCC, New York, NY, USA. [13]Computational and Systems Biology Program, MSKCC, New York, NY, USA. [14]Adult Bone Marrow Transplantation Service, MSKCC, New York, NY, USA. [15]Immunology Program, Sloan Kettering Institute, MSKCC, New York, NY, USA. [16]Institute for Computational Biomedicine, Weill Cornell Medicine, New York, NY, USA. [17]Parker Institute for Cancer Immunotherapy, New York, NY, USA. ✉e-mail: klebanoc@mskcc.org

https://doi.org/10.1038/s43018-025-01009-x

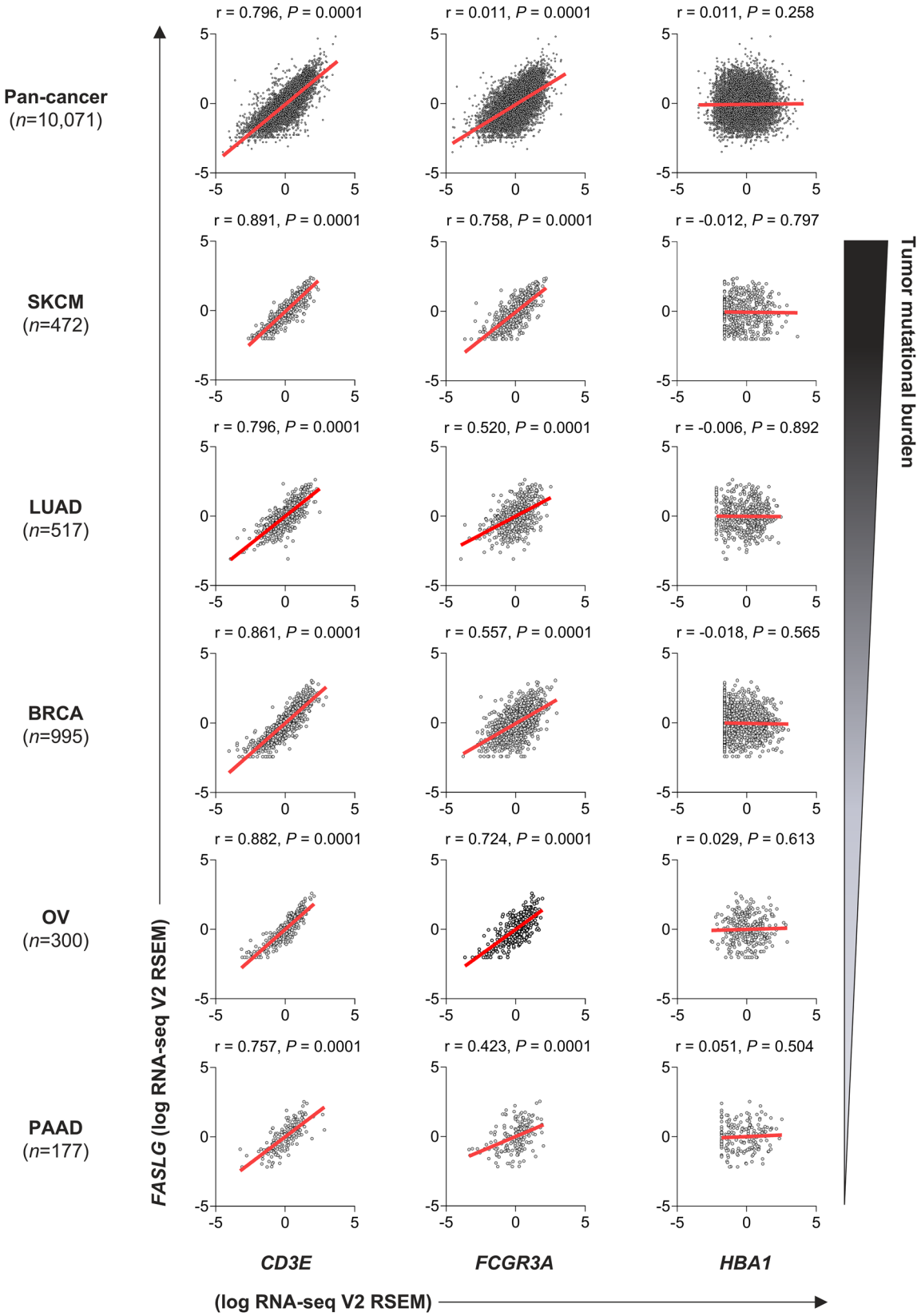

Extended Data Fig. 1 | Patient-level correlations between expression of T and NK cell-associated genes and *FASLG* using bulk RNA sequencing. Correlation between *CD3E*, *FCGR3A* (the gene encoding CD16A), *HBA1* (hemoglobin subunit α1), representing T, NK, and red blood cells as non-lymphocyte controls respectively, and *FASLG* using patient-level data obtained from The Cancer Genome Atlas (TCGA). Red line represents a simple linear regression through the data points. SKCM = skin cutaneous melanoma, BRCA = breast invasive carcinoma, OV = ovarian serous cystadenocarcinoma, PAAD = pancreatic adenocarcinoma. r = Pearson correlation coefficient, RSEM = RNA-Seq by Expectation Maximization, ns = not significant. *P* values calculated using a two-tailed F-test.

https://doi.org/10.1038/s43018-025-01009-x

a.

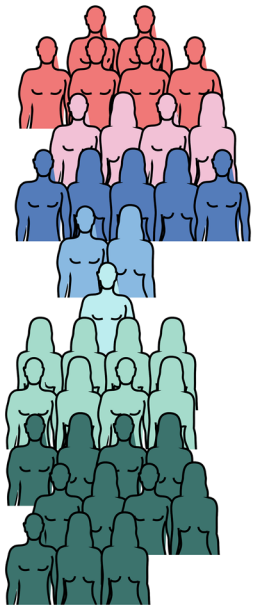

Cancer	(*n*)	Age	Cells (*n*)	Reference (PMID)
B-ALL	6	n.d.	26,062	32415257
CLL	4	48-64	12,927	31996669
LUAD/ LUSC	5	n.d.	24,759	31033233; 34290408
KIRC	2	57-62	23,130	30550791
SKCM	1	65	11,996	32539073
COAD/ READ	8	42-83	31,877	32302573
UM	11	44-96	103,703	31980621
	37			

b.

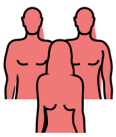

Cancer	(*n*)	Age	Treatment	Cells (*n*)	Reference (PMID)
B-ALL	3	27-77	1928ζ (SJ25C)	30,968	29385376

c.

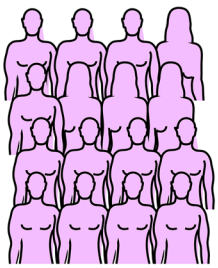

Cancer	(*n*)	Age	Treatment	Cells (*n*)	Reference (PMID)
DLBC	16	38-77	1928ζ (FMC63)	602,577	36097221

d.

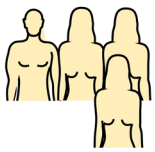

Cancer	(*n*)	Age	Cells (*n*)	Reference (PMID)
Healthy donor	4	n.d.	10,355	32415257, 30550791

Total sample size: *n*=60

Extended Data Fig. 2 | Overview of patient samples used to generate a single-cell atlas of *FASLG* expression by endogenous and CAR-engineered cells. Summary of (**a**) cell therapy naive patients with cancer, (**b**,**c**) patients with cancer treated with one of two distinct 1928ζ CARs, and (**d**) healthy donors analyzed using single-cell techniques to generate a *FASLG* expression atlas. Pictographs and tables display the sample size for each cancer cohort, gender distribution, age range, total number of single-cells analyzed, and reference to the primary datasets. B-ALL = B cell acute lymphoblastic leukemia; CLL = chronic lymphocytic leukemia; COAD = colon adenocarcinoma; DLBC = diffuse large B cell lymphoma; KIRC = kidney renal clear cell carcinoma; LUAD = lung adenocarcinoma; LUSC = lung squamous cell carcinoma; READ = rectal adenocarcinoma; SKCM = skin cutaneous melanoma; UM = uveal melanoma. n.d. = no data.

https://doi.org/10.1038/s43018-025-01009-x

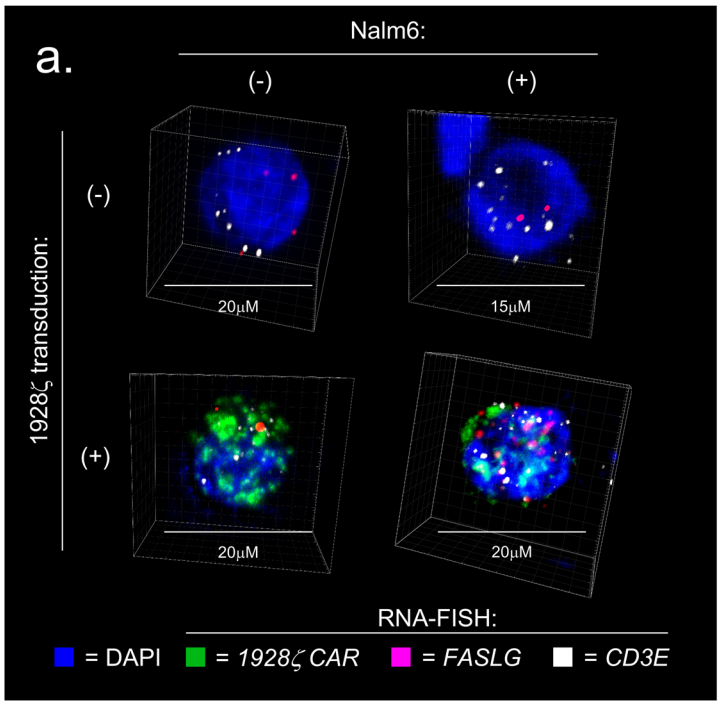

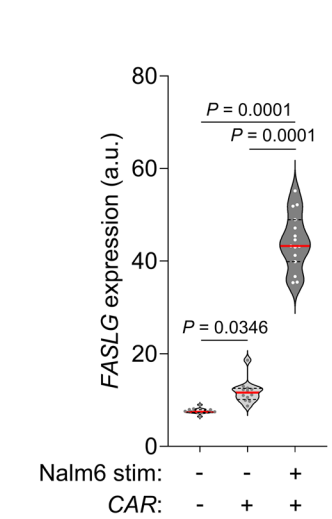

Extended Data Fig. 3 | Quantification of *FASLG* expression by 1928ζ CAR-expressing T cells following in vitro co-culture with CD19$^+$ leukemia cells using RNA in situ hybridization. (**a**) Representative immunofluorescent confocal images and (**b**) summary violin plots quantifying *FASLG* mRNA expression by nontransduced or 1928ζ CAR-expressing T cells at rest or 24 h following *in vitro* co-culture with CD19$^+$ Nalm6 B-ALL. Samples were co-hybridized with DAPI (blue) and multiplexed RNA-FISH probes specific for the mRNA sequence of the CAR's single-chain variable fragment (scFv) (green), *CD3E* mRNA (white), and *FASLG* mRNA (red). Data shown is representative of results from $n = 12$, $n = 13$, and $n = 15$ gated regions from nontransduced T cells, CAR-T cells alone, and CAR-T cells co-cultured with Nalm6 cells, respectively. T cells were derived from $n = 2$ healthy donors. Violin distributions are centered around the median (red horizontal line) with quartiles ranges displayed above and below (dashed horizontal lines). The maxima and minima are represented by the top and bottom of each plot. Each dot represents mean *FASLG* mRNA expression within a particular cell type from a region of interest. *P*-values calculated using a one-way ANOVA with a Šídák's multiple comparisons test. a.u. = arbitrary fluorescence units.

https://doi.org/10.1038/s43018-025-01009-x

a.

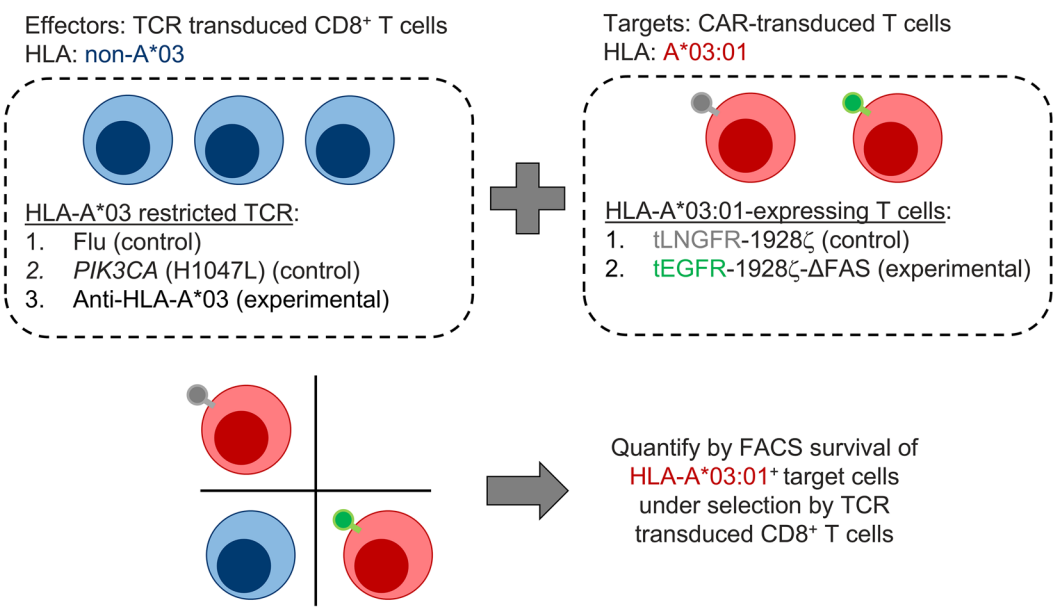

b.

TCR ID	Restricting HLA allele	Epitope	TRAV	TRAJ	TRBV	TRBJ	CDR3α / CDR3β
RG4382-5	A*03:01	undefined	TRAV12-3*01	TRAJ12*01	TRBV12-3*01	TRBJ1-1*01	CAMSDPRSSYKLIF / CASSPGGTEAFF

c.

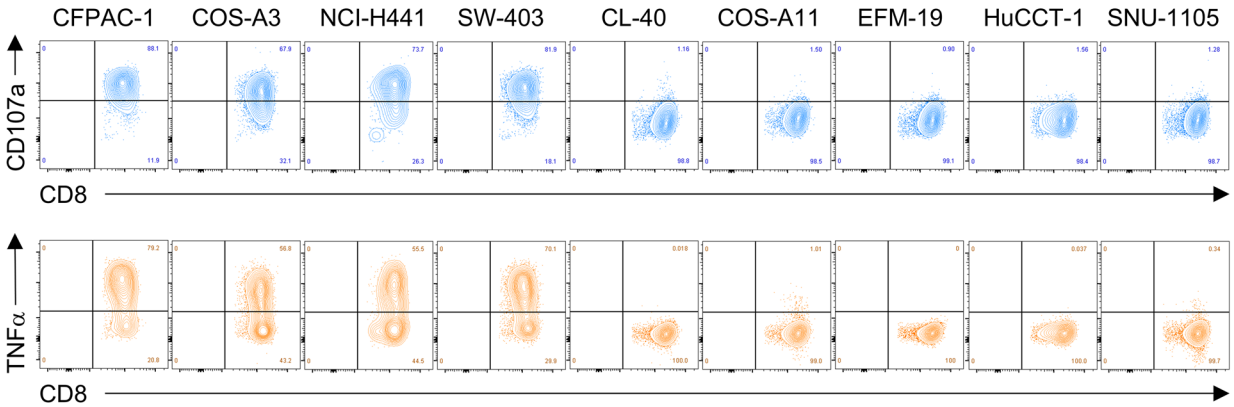

d.

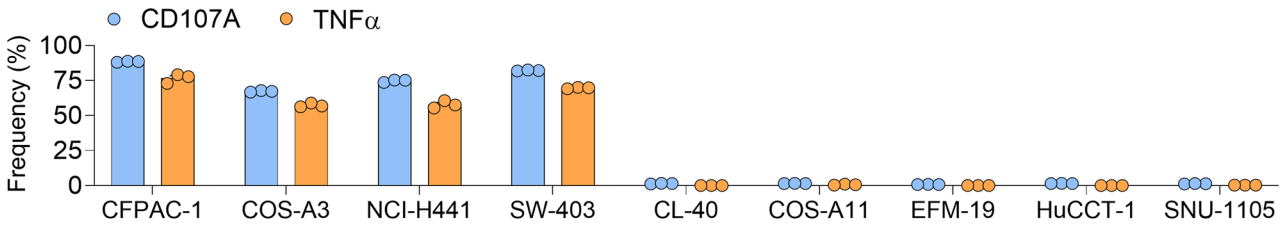

HLA-A (1)	03:01	03:01	03:01	03:01	11:01	11:01	29:02	11:01	11:01
HLA-A (2)	02:01	03:01	02:01	02:05	11:01	11:01	33:03	11:01	24:02

Extended Data Fig. 4 | See next page for caption.

https://doi.org/10.1038/s43018-025-01009-x

Extended Data Fig. 4 | Experimental design and reagents for testing whether ΔFAS protects against TCR-mediated rejection of allogeneic lymphocytes. (**a**) Graphical overview of an experimental design to test whether ΔFAS coexpression protects CAR-T cells from elimination by allo-reactive T cells. $CD8^+$ T cells from a non-HLA-A*03 donor were transduced either with control HLA-A*03:01-restricted TCRs or TCR (RG4382-5), an allo-reactive TCR that recognizes HLA-A*03^+ cells in a peptide agnostic manner. TCR transduced T cells were co-cultured with a ~ 1:1 mixture of HLA-A*$03:01^+$ T cells transduced with tLNGFR-1928ζ or tEGFR-1928ζ-ΔFAS at a 10:1 effector-to-target-ratio. (**b**) Table listing the *TRAV*, *TRAJ*, *TRBV*, *TRBJ*, and CDR3 sequences for a TCR (RG4382-5) that confers allogeneic recognition of HLA-A*$03:01^+$ cells. (**c**) Representative FACS plots and (**d**) summary bar graphs of CD107a and TNFα expression by non-HLA-A*03 $CD8^+$ T cells transduced with the RG4382-5 TCR and co-cultured with the indicated cells lines. The HLA-A haplotype of each cell line is listed as a table below. Numbers within each FACS plot and bar graph indicate the frequency of CD107a or TNFα producing T cells after pre-gating on $live^+mTCR^+CD8^+$ cells. Bar graphs displayed as mean ± SEM ($n = 3$ biologically independent samples).

https://doi.org/10.1038/s43018-025-01009-x

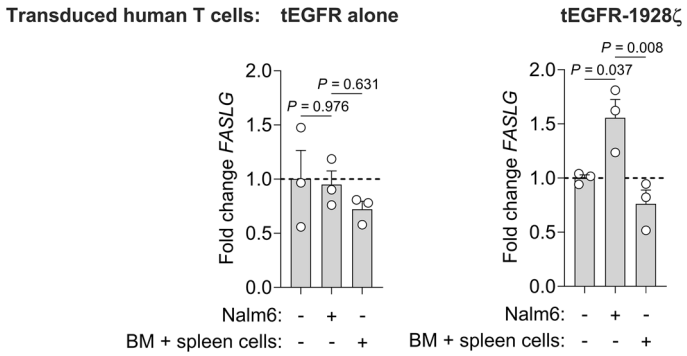

Extended Data Fig. 5 | Transduced human T cells do not upregulate *FASLG* when co-cultured with murine splenocytes and bone marrow cells. Fold change in *FASLG* expression levels by human T cells transduced either with tEGFR alone (left panel) or tEGFR-1928ζ (right panel) and cultured alone or together either with Nalm6 cells or a 1:1 mixture of murine bone marrow (BM) cells and splenocytes. T cells were cultured for 24 h under indicated conditions before isolation by positive selection using an anti-EGFR antibody. *FASLG* expression was quantified by qPCR and normalized to *GAPDH*. Data shown as mean ± s.e.m. using donor cells obtained from $n = 3$ unique mice. *P* values calculated using a one-way ANOVA with a Šídák's multiple comparisons test.

https://doi.org/10.1038/s43018-025-01009-x

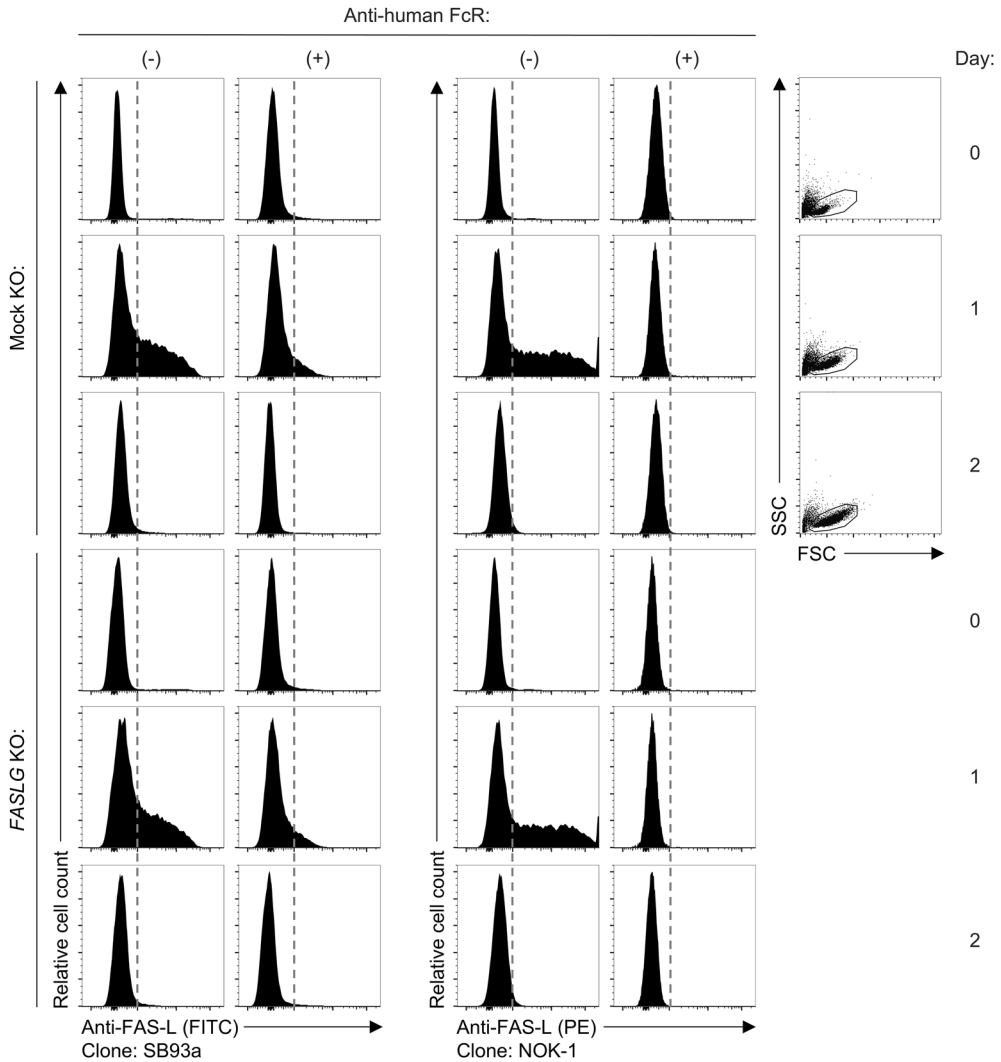

Extended Data Fig. 6 | Commercially available FACS antibodies fail to specifically detect FAS ligand expression on the surface of resting and activated human T cells. A bulk population of human T cells was activated using ImmunoCult and left untreated as controls (mock KO) or underwent *FASLG* gene editing using CRISPR/Cas9 (*FASLG* KO). After one week, T cells were stained with the indicated fluorochrome-conjugated FAS-L antibody clone at rest or at indicated time points following re-activation. Anti-FAS-L antibody staining was performed in the absence or presence of a FcR blocking antibody. Data are representative of three individually cultured samples per donor and was repeated twice with similar results using two separate donors. Vertical lines define the negative staining T cell population at rest for each fluorescent channel.

https://doi.org/10.1038/s43018-025-01009-x

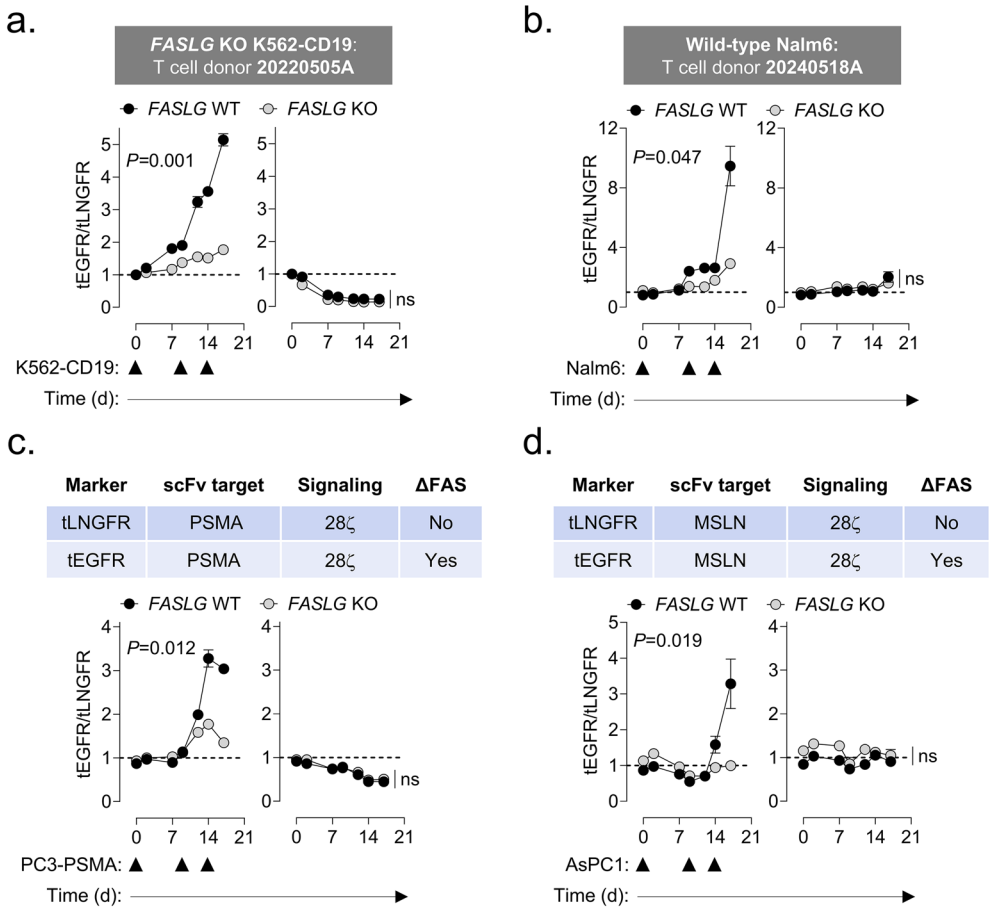

Extended Data Fig. 7 | ΔFAS enhances the competitive fitness of CAR-T cells following repetitive tumor cell exposure in a *FASLG*-dependent manner across donors and cancer types. (**a,b**) Relative antigen-driven in vitro expansion of control and *FASLG* KO 1928ζ CAR-T cells ± ΔFAS coexpression following repetitive exposure to different hematologic malignancies. (**a**) CAR-T cells derived from donor 20240412 A that express (tEGFR$^+$) or do not express (tLNGFR$^+$) ΔFAS were combined in ~1:1 ratio on day 0 and serially restimulated at indicated time points with K562-CD19 *FASLG* KO leukemia cells (left panel) or left unstimulated as controls (right panel). (**b**) Same as (**a**) but CAR-T cells were generated from donor 20240518 A and restimulated with wild-type (WT) Nalm6 leukemia cells. (**c,d**) Relative antigen-driven in vitro expansion of control versus *FASLG* KO (PSMA)28ζ or (MSLN)28ζ CAR-T cells ± ΔFAS coexpression following repetitive exposure to different solid malignancies. (**c**) (PSMA)28ζ CAR-T cells that express (tEGFR$^+$) or do not express (tLNGFR$^+$) ΔFAS were combined in ~1:1 ratio on day 0 and serially restimulated at indicated time points with PC3-PSMA (left panel), a human prostate cancer cell line PC3 transduced with PSMA, or left unstimulated as controls (right panel). (**d**) Same as (**c**) but using a (MSLN)28ζ CAR serially restimulated with AsPC1, a human pancreatic cancer cell line that naturally expresses mesothelin. Data in all panels reflect the ratio of tEGFR/tLNGFR T cells measured by FACS at indicated time points and is displayed as the mean ratio ± s.e.m. ($n = 3$ biologically independent samples). Groups were compared using a paired two-tailed Student's *t*-test for accumulated differences between each time point. ns, not significant ($P > 0.05$).

https://doi.org/10.1038/s43018-025-01009-x

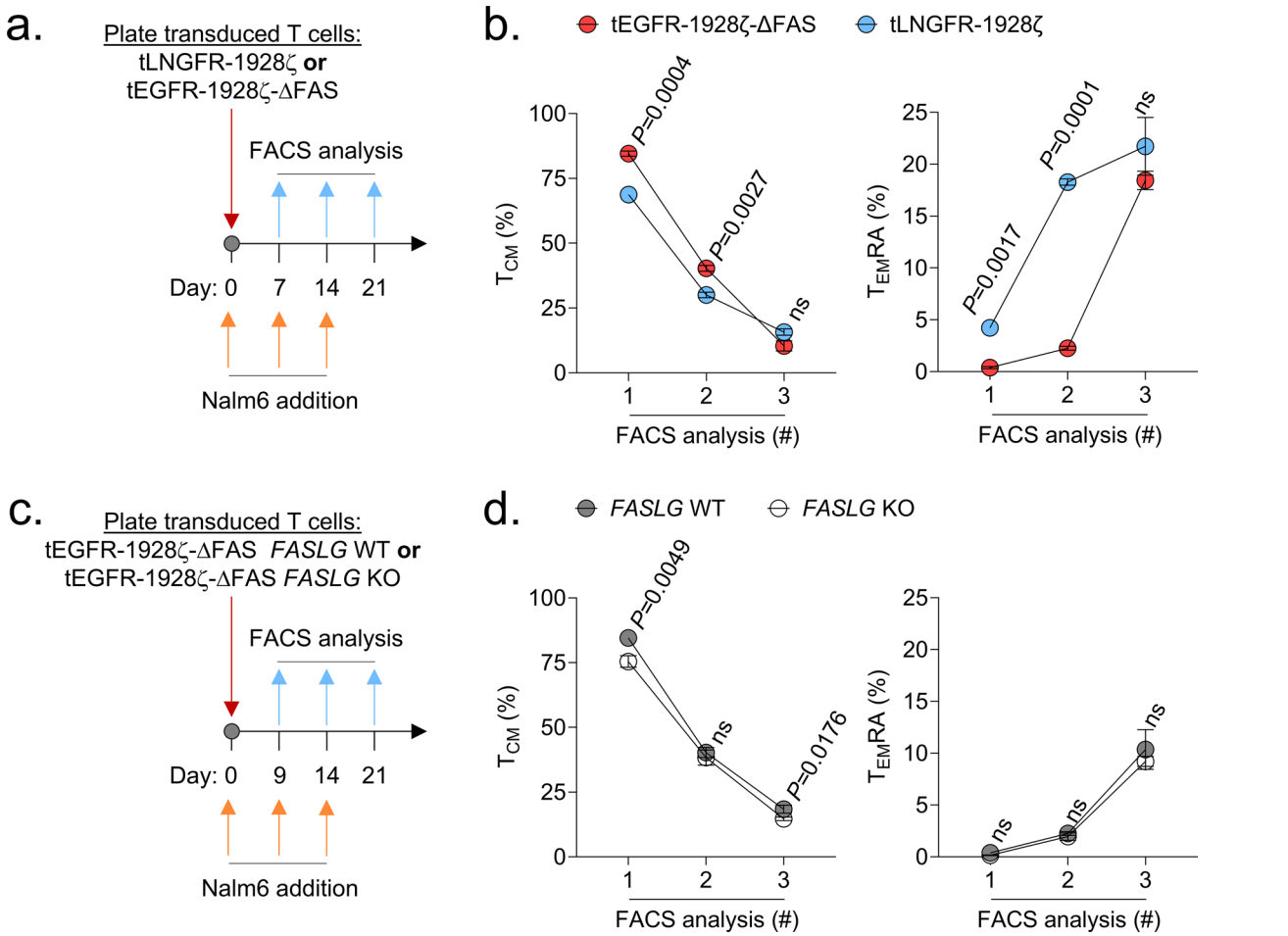

Extended Data Fig. 8 | Disabling FAS signaling restrains terminal differentiation of CAR-T cells following serial antigen encounter. (**a**) Experimental design for testing the impact of ΔFAS coexpression on the distribution of memory T cell subsets following serial engagement of 1928ζ CAR-T cells with Nalm6 B-ALL cells. T cells transduced either with tLNGFR-1928ζ or tEGFR-1928ζ-ΔFAS were individually co-cultured at a 1:2 ratio with Nalm6 cells. Beginning nine days after the first exposure to tumor cells, Nalm6 cells were re-added to the co-culture every five to six days for a total of three rounds of stimulation. Following each round, an aliquot of cells was harvested and analyzed by FACS. (**b**) Summary of the distribution of T_{CM} ($CD45RA^{-}CD45RO^{+}CCR7^{+}$) and $T_{EM}RA$ ($CD45RA^{+}CD45RO^{+}CCR7^{-}$) phenotype CAR-T cells following one, two, or three rounds of stimulation with Nalm6 cells. (**c**) Experimental design for testing the impact of T cell-derived *FASLG* on the distribution of memory T cell subsets following serial engagement of tEGFR-1928ζ-ΔFAS CAR-T cells with Nalm6 B-ALL cells. *FASLG* was knocked out (KO) of transduced T cells using CRISPR/Cas9 or left untreated as controls. Time points were identical to those shown in (**a**). (**d**) Summary of the distribution of T_{CM} and $T_{EM}RA$ phenotype CAR-T cells following one, two, or three rounds of stimulation with Nalm6 cells. Data in panels (**b**) and (**d**) is displayed as the mean ± s.e.m. of the indicated memory subset ($n = 3$ biologically independent samples after gating on transduced T cells identified by EGFR or LNGFR expression). Groups were compared using a paired two-tailed *t*-test. ns = not significant.

https://doi.org/10.1038/s43018-025-01009-x

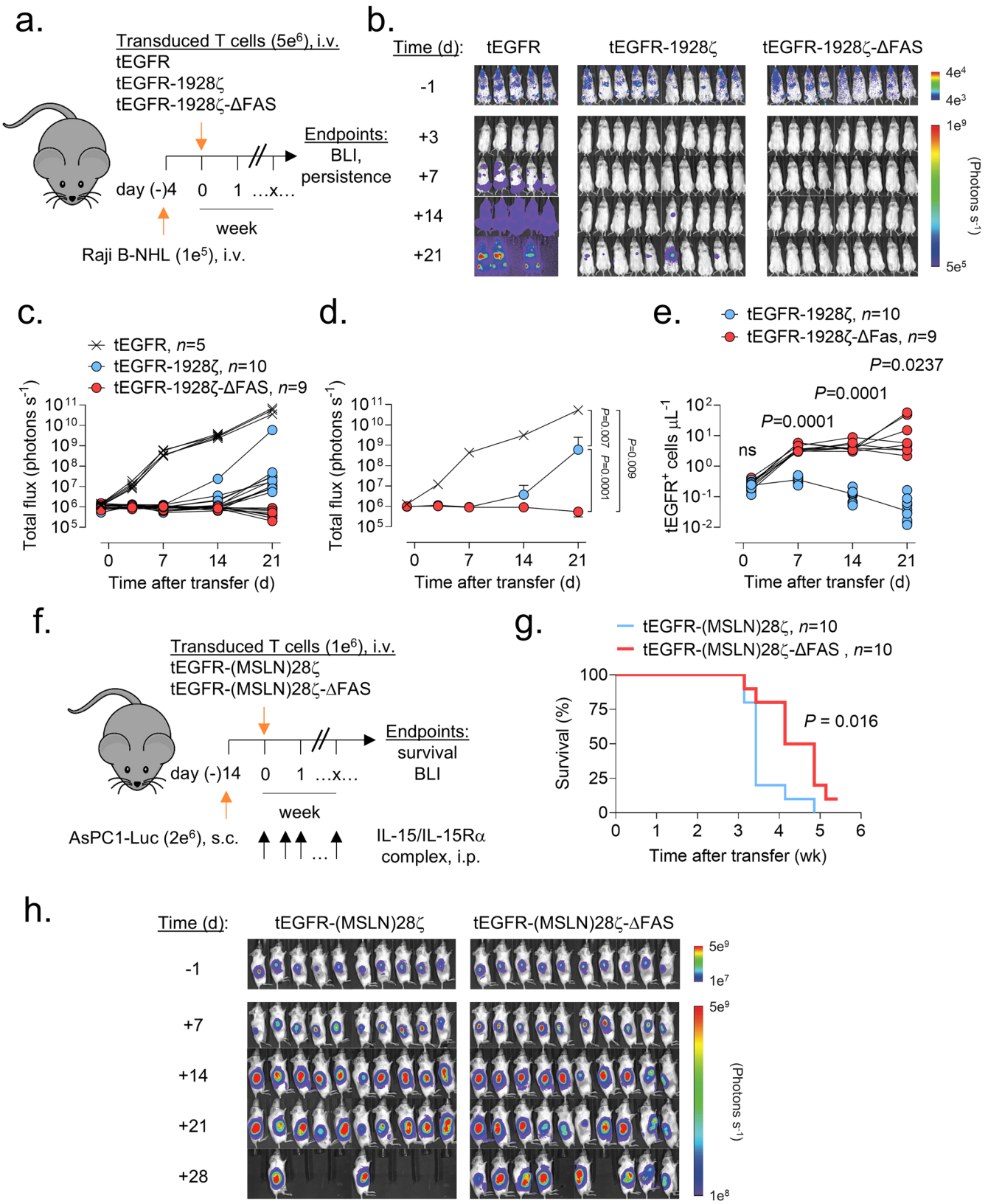

Extended Data Fig. 9 | See next page for caption.

https://doi.org/10.1038/s43018-025-01009-x

Extended Data Fig. 9 | Disabling FAS signaling enhances CAR-T cell persistence and antitumor efficacy in the setting of B cell Non-Hodgkin lymphoma and a solid malignancy. (**a**) Experimental design to compare the in vivo antitumor efficacy and persistence of human T cells expressing a 1928ζ CAR ± a FAS dominant negative receptor (ΔFAS) against four day established Raji-luciferase (Luc) B cell non-Hodgkin lymphoma (B-NHL). (**b**) Bioluminescence imaging, (**c**) individual, and (**d**) summary curves of tumor burden as a function of time using $n = 5$ (tEGFR), $n = 10$ mice (tEGFR-1928ζ), or $n = 9$ (tEGFR-1928ζ-ΔFAS) mice per group. Data in (**d**) displayed as mean ± standard deviation. Tumor burden at the final time point (d21) was compared using an unpaired one-tailed Mann-Whitney test. (**e**) Quantification of the absolute number of circulating CAR-T cells (cells mL^{-1}) in the peripheral blood as a function of time in Raji B-NHL bearing mice. Mice received by IV adoptive transfer $5e^6$ tEGFR-1928ζ or tEGFR-1928ζ-ΔFAS CAR-T cells. Each symbol represents values from individually evaluated mice. *P* values calculated based on comparison of ΔFAS-expressing Vs. not expressing CAR-T cells at each time point using an unpaired, two-sided, *t*-test. (**f**) Experimental design for comparing the in vivo antitumor efficacy of human T cells transduced with a (MSLN)28ζ CAR ± ΔFAS against subcutaneous (s.c.) 14 day established AsPC1-luciferase (Luc) pancreatic cancer tumors. All mice received twice-weekly intraperitoneal (i.p.) injections of 1 μg of IL-15 pre-complexed with IL-15Rα-Fc (1:1 M) and a single intravenous (i.v.) injection of $1e^6$ human CAR^+ T cells. (**g**) Survival curves and (**h**) bioluminescent imaging of treated mice. Survival data is plotted as a Kaplan–Meier survival curve with groups statistically compared using a log-rank test. wk = week.

https://doi.org/10.1038/s43018-025-01009-x

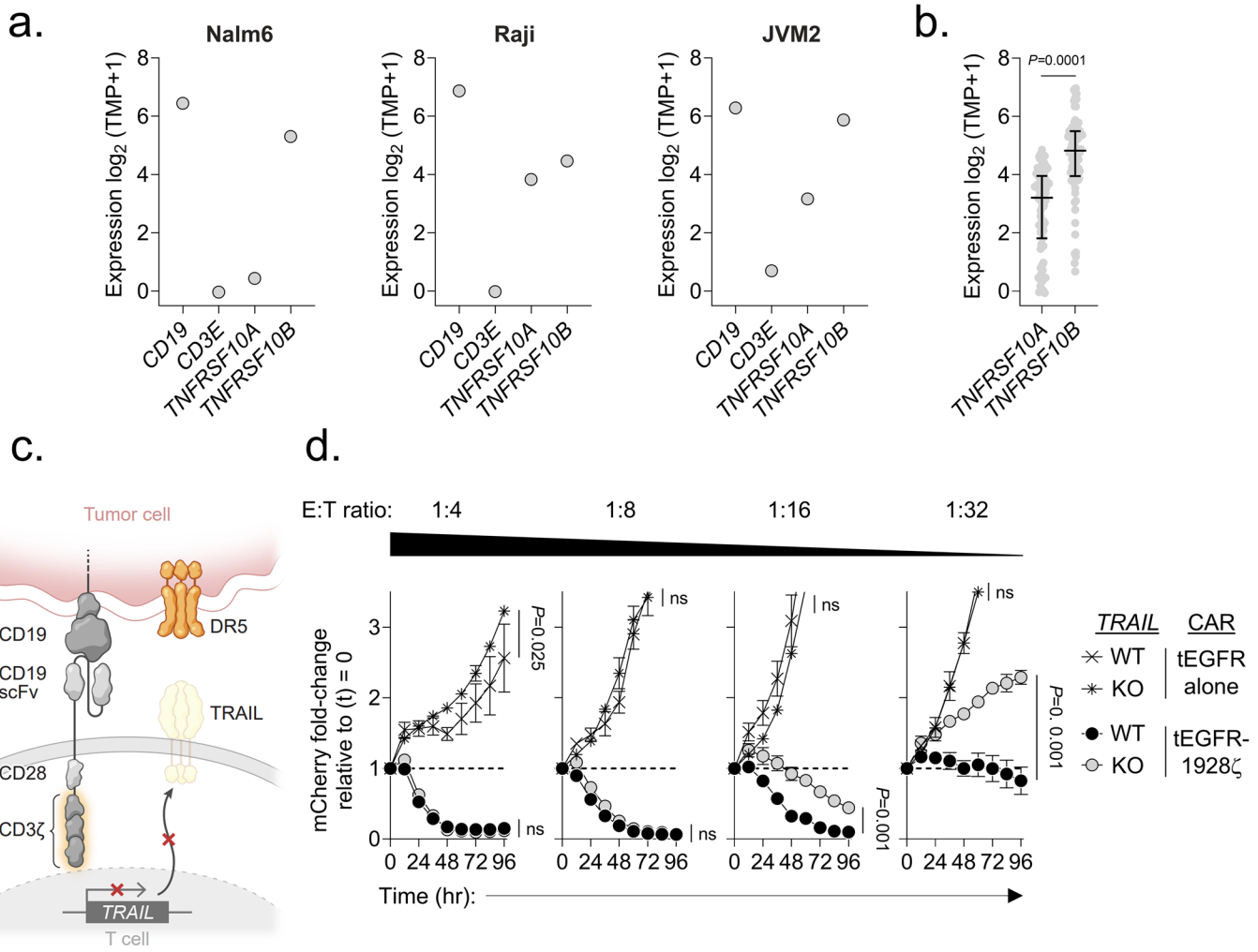

e.

CAR	*TRAIL*	*TRAIL* Indel freq. ± s.e.m.
tEGFR	WT	0%
tEGFR	KO	59.7% ± 1.2%
tEGFR-1928ζ	WT	0%
tEGFR-1928ζ	KO	58.3 ± 0.5%

Extended Data Fig. 10 | Knockout of *TRAIL* in 1928ζ CAR-T cells significantly impairs antitumor cytolytic activity. (**a**) RNA-seq values for *CD19*, *CD3E*, *TNFRSF10A* (the gene encoding DR4) and *TNFRSF10B* (the gene encoding DR5) in Nalm6, Raji, and JVM2 B cell malignancy cell lines. (**b**) Scatter-plot of *TNFRSF10A* and *TNFRSF10B* RNA-seq values from $n = 83$ B cell lines featured in the Cancer Cell Line Encyclopedia (CCLE). Horizontal line represents the median value while the vertical bars represent the interquartile range. *P* value calculated using an unpaired two-tailed Student's *t*-test. TPM = transcript per million. (**c**) Schematic for the CRISPR/Cas9-mediated knockout (KO) of *TRAIL* in human $CD8^+$ T cells expressing a 1928ζ CAR. (**d**) Cytolytic activity of *TRAIL* KO versus wild-type (WT)-*TRAIL* 1928ζ CAR-T cells or T cells transduced with tEGFR alone against Nalm6/NLS–mCherry at indicated effector-to-target (E:T) ratios. Data shown as mean ± s.e.m. ($n = 3$ biologically independent samples). Statistical comparisons performed using a one-way ANOVA. ns = not significant, $P > 0.05$. (**e**) Table displaying the measured frameshift insertion-deletion (Indel) frequency in *TRAIL* for each T cell group used in the cytolytic assay. Data shown as mean ± s.e.m. ($n = 3$ technical replicates from 1 experiment, repeated with similar results using n = 2 donors).

nature portfolio

Corresponding author(s): Christopher A. Klebanoff, M.D.

Last updated by author(s): May 22, 2025

Reporting Summary

Nature Portfolio wishes to improve the reproducibility of the work that we publish. This form provides structure for consistency and transparency in reporting. For further information on Nature Portfolio policies, see our Editorial Policies and the Editorial Policy Checklist.

Statistics

For all statistical analyses, confirm that the following items are present in the figure legend, table legend, main text, or Methods section.

n/a	Confirmed
☐	☒ The exact sample size (*n*) for each experimental group/condition, given as a discrete number and unit of measurement
☐	☒ A statement on whether measurements were taken from distinct samples or whether the same sample was measured repeatedly
☐	☒ The statistical test(s) used AND whether they are one- or two-sided *Only common tests should be described solely by name; describe more complex techniques in the Methods section.*
☒	☐ A description of all covariates tested
☐	☒ A description of any assumptions or corrections, such as tests of normality and adjustment for multiple comparisons
☐	☒ A full description of the statistical parameters including central tendency (e.g. means) or other basic estimates (e.g. regression coefficient) AND variation (e.g. standard deviation) or associated estimates of uncertainty (e.g. confidence intervals)
☐	☒ For null hypothesis testing, the test statistic (e.g. *F*, *t*, *r*) with confidence intervals, effect sizes, degrees of freedom and *P* value noted *Give P values as exact values whenever suitable.*
☒	☐ For Bayesian analysis, information on the choice of priors and Markov chain Monte Carlo settings
☒	☐ For hierarchical and complex designs, identification of the appropriate level for tests and full reporting of outcomes
☐	☒ Estimates of effect sizes (e.g. Cohen's *d*, Pearson's *r*), indicating how they were calculated

Our web collection on statistics for biologists contains articles on many of the points above.

Software and code

Policy information about availability of computer code

Data collection	Flow cytometry data were collected with BD FACS DIVAv9.2. RNA-FISH data were collected with Leica Bond RX version 7. Confocal imaging done on ZenBlack 2.3SP1. Western blot data were collected with LICOR Odyssey CLx with Image Studio 5.2. Real-time cell imaging data were collected with Incucyte 2023A. Bio-luminescence data were collected with IVIS Imaging System. Real-time PCR data were collected with ABI QuantStuidio 5.
Data analysis	Flow cytometry data were analyzed on Flowjo 10.6.2. RNA-FISH data were analyzed on QuPath 0.5.0, 3D reconstruction were done on Zen lite-Blue version 2.6 and Imaris version 9.5 imaging software. Western blot data were analyzed on LICOR Odyssey CLx with Image tudio5.2. Real-time cell imaging data were analyzed on Incucyte Basic Analysis Software 2023A. Bio-luminescence data were analyzed on Living Image Software 2.6. Real-time PCR data were analyzed on Thermo Fisher Connect DA2. Statistic analysis were done with SPICE 6.0 and GraphPad Prism 10. Code is available at https://github.com/abcwcm/Yi2024.

For manuscripts utilizing custom algorithms or software that are central to the research but not yet described in published literature, software must be made available to editors and reviewers. We strongly encourage code deposition in a community repository (e.g. GitHub). See the Nature Portfolio guidelines for submitting code & software for further information.

Data

Policy information about availability of data

All manuscripts must include a data availability statement. This statement should provide the following information, where applicable:

- Accession codes, unique identifiers, or web links for publicly available datasets
- A description of any restrictions on data availability
- For clinical datasets or third party data, please ensure that the statement adheres to our policy

Previously published bulk RNA-seq data sets (pan-cancer, skin cutaneous melanoma, lung adenocarcinoma, breast invasive carcinoma, ovarian serous cystadenocarcinoma, and pancreatic adenocarcinoma) resulting from the TCGA Research Network (https://www.cancer.gov/tcga) were re-analyzed using cBioPortal78. Publicly available single-cell RNA sequence (scRNA-seq) datasets from patients who had not received prior CAR-T therapy were assembled from the eight studies listed in Extended Data Fig. 2. Raw count matrices were retrieved from the Gene Expression Omnibus (GEO) using the following accession numbers: GSE132509, GSE111014, GSE117570, GSE111360, GSE148190, GSE146771, GSE176021, and GSE139829. When available, cell annotations were retrieved from TISCH79. Raw count matrices for publicly available scRNA-seq datasets from patients who had prior 1928z CAR-T therapy are available from GSE197268. Count matrices from whole genome CRISPR/Cas9 screens are available in supplementary tables of the related publication (ref. 42) or GSE130663. The remaining data are available within the Article, Supplementary Information and Source Data file and/or from the corresponding author on request. Source data are provided in this paper.

Research involving human participants, their data, or biological material

Policy information about studies with human participants or human data. See also policy information about sex, gender (identity/presentation), and sexual orientation and race, ethnicity and racism.

Reporting on sex and gender	Patients and donors were not selected in regard of sex and gender. Sex was self-reported.
Reporting on race, ethnicity, or other socially relevant groupings	Patients and donors were not selected in regard of race, ethnicity or other socially relevant groupings.
Population characteristics	Population characteristics was described in Extended Data Fig. 2.
Recruitment	Patient recruitment information was described in ClinicalTrials NCT01044069. Human primary lymphocytes were accquired from donors recruited by Stemcell Technologies and New York Blood Center.
Ethics oversight	Human patient samples were collected after obtaining informed consent and with approval from the human studies review board at MSKCC (IRB# 09-114 (ClinicalTrials.gov ID:01044069)) as part of a clinical investigation conducted according to the principles of the Declaration of Helsinki. Participation was voluntary and the patients did not receive compensation. For T cell preparations, buffy coats were obtained from the New York Blood Center and STEMCELL Technologies from healthy volunteer donors after written informed consent was obtained using IRB approved consent forms.

Note that full information on the approval of the study protocol must also be provided in the manuscript.

Field-specific reporting

Please select the one below that is the best fit for your research. If you are not sure, read the appropriate sections before making your selection.

☒ Life sciences ☐ Behavioural & social sciences ☐ Ecological, evolutionary & environmental sciences

For a reference copy of the document with all sections, see nature.com/documents/nr-reporting-summary-flat.pdf

Life sciences study design

All studies must disclose on these points even when the disclosure is negative.

Sample size	Sample sizes were given in the main text, figure legends or methods. No statistical methods were used to predetermine sample sizes. Typical group size is 10 mice per group. At least 5 mice sacrificed to assess cell counts at different time points.
Data exclusions	No data were excluded from the analysis, except the samples disqualified RNA-FISH or PCR quality controls which had no readouts.
Replication	In vitro experimental data were generated from two or more independent experiments containing n=3 biologically independent samples . All attempts at replication were successful. For in vivo mouse experiments, treatment groups had n=5-15 mice per condition, and control groups had n=5-10 mice as described in figures and figure legends.
Randomization	Animals used in this study were all of the same breed and genotype and randomized for grouping by the veterinary staff.
Blinding	Cell injection, drug administration and data acquisition were performed by investigators blinded to treatment groups. Analysis were

Blinding

performed by researches who were not blinded to the experiments as data was quantitative using a well-controlled system involving established tumor models from cell lines.

Reporting for specific materials, systems and methods

We require information from authors about some types of materials, experimental systems and methods used in many studies. Here, indicate whether each material, system or method listed is relevant to your study. If you are not sure if a list item applies to your research, read the appropriate section before selecting a response.

Materials & experimental systems

n/a	Involved in the study
☐	☒ Antibodies
☐	☒ Eukaryotic cell lines
☒	☐ Palaeontology and archaeology
☐	☒ Animals and other organisms
☒	☐ Clinical data
☒	☐ Dual use research of concern
☒	☐ Plants

Methods

n/a	Involved in the study
☒	☐ ChIP-seq
☐	☒ Flow cytometry
☒	☐ MRI-based neuroimaging

Antibodies

Antibodies used

Antibody name (Clone, Fluorochrome) (Vendor, Cat#), Dilution as v/v
anti-mouse F(ab')2 (polyclonal, AF647) (Jackson ImmunoResearch, Cat# 115-605-072), 5%
anti-human CCR7 (G043H7, AF647) (Biolegend, Cat# 353218), 5%
anti-human EGFR (AY13, BV421) (Biolegend, Cat#352911), 0.5%
anti-human EGFR (AY13, PE) (Biolegend, Cat#, 352904), 0.2%
anti-human Fas-L (SB92a, FITC) (Thermo Fisher, Cat# A15381), 20%
anti-human Fas-L (NOK-1, PE) (Biolegend, Cat# 306407), 20%
anti-human Fc receptor (Fc1, n/a) (BD, Cat# 564220), 10%
anti-human LNGFR (C40-1457, AF647) (BD, Cat# 560326), 3%
anti-human LNGFR (C40-1457, PE) (BD, Cat# 560927),3%
anti-human Fas (DX2, PE Cy5) (Biolegend, Cat# 305610), 2%
anti-human Fas (DX2, APC Cy7) (Biolegend, Cat# 305636), 3%
anti-human CD3 (OKT3, APC) (Biolegend, Cat# 317318), 5%
anti-human CD3 (OKT3, BV785) (Biolegend, Cat# 317330), 3%
anti-human CD4 (SK3, SB780) (Thermo Fisher, Cat# 78-0047-42), 5%
anti-human CD8a (RPA-T8, PE Cy7) (Biolegend, Cat# 301012), 2%
anti-human CD14 (HCD14, FITC) (Biolegend, Cat# 325604), 3%
anti-human CD19 (HIB19, BV650) (Biolegend, Cat# 302238), 3%
anti-human CD45 (HI30, PE Cy7) (Biolegend, Cat# 304016), 3%
anti-human CD45RA (HI100, PerCP Cy5.5) (Biolegend, Cat# 304122), 5%
anti-human CD45RO (UCHL1, APC eFluor780) (ThermoFisher, Cat# 47-0457-42), 5%
anti-human CD56 (5.1H11, APC) (Biolegend, Cat# 981204), 3%
anti-human CD56 (5.1H11, PE) (Biolegend, Cat# 362524), 3%
anti-human CD107a (H4A3, BV650) (BD, Cat# 328638), 5%
anti-human HLA-A3 (GAP.A3, PE) (Thermo Fisher, Cat# 12-57542), 3%
anti-mouse TCRβ (H57-597, PerCP Cy5.5) (Thermo Fisher, Cat# 45-5961-82), 3%
anti-human IFN-γ (B27, FITC) (BD, Cat# 554700), 5%
anti-human TNFα (Mab11, PerCP Cy5.5) (Thermo Fisher, Cat# 45-7349-42), 20%
anti-human IL-2 (MQ1-17H12, PE Cy7) (Thermo Fisher, Cat# 25-7029-42), 20%

Validation

Validation of each antibody is provided below as well as in Supplementary Figures 1 and 2.
F(ab')2 https://www.jacksonimmuno.com/catalog/products/115-605-072

CCR7 https://www.biolegend.com/en-us/products/alexa-fluor-647-anti-human-cd197-ccr7-antibody-7538

EGFR https://www.biolegend.com/en-us/products/brilliant-violet-421-anti-human-egfr-antibody-8621

EGFR https://www.biolegend.com/en-us/products/pe-anti-human-egfr-antibody-7432

Fas-L https://www.thermofisher.com/antibody/product/CD178-Antibody-clone-SB93a-Monoclonal/A15381

Fas-L https://www.biolegend.com/en-ie/products/pe-anti-human-cd178-fasl-antibody-806

Fc receptor https://www.bdbiosciences.com/en-us/products/reagents/flow-cytometry-reagents/research-reagents/single-color-antibodies-ruo/human-bd-fc-block.564219?tab=product_details

LNGFR https://www.bdbiosciences.com/en-us/products/reagents/flow-cytometry-reagents/research-reagents/single-color-antibodies-ruo/alexa-fluor-647-mouse-anti-human-cd271.560326?tab=product_details

LNGFR	https://www.bdbiosciences.com/en-us/products/reagents/flow-cytometry-reagents/research-reagents/single-color-antibodies-ruo/pe-mouse-anti-human-cd271.560927?tab=product_details
FAS	https://www.biolegend.com/en-us/products/pe-cyanine5-anti-human-cd95-fas-antibody-644
FAS	https://www.biolegend.com/en-us/products/apc-cyanine7-anti-human-cd95-fas-antibody-12141
CD3	https://www.biolegend.com/en-us/products/apc-anti-human-cd3-antibody-6198
CD3	https://www.biolegend.com/en-us/products/brilliant-violet-785-anti-human-cd3-antibody-7977
CD4	https://www.thermofisher.com/antibody/product/CD4-Antibody-clone-SK3-SK-3-Monoclonal/78-0047-42
CD8a	https://www.biolegend.com/en-us/products/pe-cyanine7-anti-human-cd8a-antibody-838
CD14	https://www.biolegend.com/en-us/products/fitc-anti-human-cd14-antibody-3951
CD19	https://www.biolegend.com/en-us/products/brilliant-violet-650-anti-human-cd19-antibody-7656
CD45	https://www.biolegend.com/en-us/products/pe-cyanine7-anti-human-cd45-antibody-1915
CD45RA	https://www.biolegend.com/en-us/products/percp-cyanine5-5-anti-human-cd45ra-antibody-4241
CD45RO	https://www.thermofisher.com/antibody/product/CD45RO-Antibody-clone-UCHL1-Monoclonal/47-0457-42
CD56	https://www.biolegend.com/en-us/products/apc-anti-human-cd56-ncam-antibody-14587
CD56	https://www.biolegend.com/en-us/products/pe-anti-human-cd56-ncam-antibody-9958
HLA-A3	https://www.thermofisher.com/antibody/product/HLA-A3-Antibody-clone-GAP-A3-Monoclonal/12-5754-42
mouse TCRβ	https://www.thermofisher.com/antibody/product/TCR-beta-Antibody-clone-H57-597-Monoclonal/45-5961-82
IFN-γ	https://www.bdbiosciences.com/en-us/products/reagents/flow-cytometry-reagents/research-reagents/single-color-antibodies-ruo/fitc-mouse-anti-human-ifn.554700?tab=product_details
TNFα	https://www.thermofisher.com/antibody/product/TNF-alpha-Antibody-clone-MAb11-Monoclonal/45-7349-42
IL-2	https://www.thermofisher.com/antibody/product/IL-2-Antibody-clone-MQ1-17H12-Monoclonal/25-7029-42

Eukaryotic cell lines

Policy information about cell lines and Sex and Gender in Research

Cell line source(s)	293T (ATCC, CRL-3216), 293GP (Takara Bio, 631458), Nalm6 (ATCC, CRL-3273), JVM-2 (ATCC, CRL-3002), Raji (ATCC, CCL-86), CFPAC-1 (ATCC, CRL-1918), NCI-H441 (ATCC, CRM-HTB-174), SW-403 (ATCC, CCL-230), CL-40 (DSMZ, ACC 535), EFM-19 (DSMZ, ACC 231), HuCCT-1 (Cytion, 300469), and SNU-1105 (KCLB, 01105) were purchased from commercial vendors. Nalm6-GFP/Luc (Nalm6 (ATCC, CRL-3273) transduced with GFP luciferase) and PC3-PSMA (PC3 (ATCC, CRL-1435) retrovirally transduced with PSMA) were obtained from the Sadelain lab (MSKCC). Raji-GFP/Luc (Raji (ATCC,CCL-86) cells modified to express GFP-FFLuc (Clontech Laboratories, Mountain View, CA)) was obtained from the Brentjens lab (MSKCC). K562-CD19 cells (K562 (ATCC, CCL-243) transduced with retroviruses encoding murine-19) was provided under MTA from the Feldman lab (NIH). K562 Clone 9 (K562 (ATCC, CCL-243) retrovirally transduced with CD64 (FcγRI), CD86 (B7-2), CD137L (4-1BBL), and truncated CD19 to create Clone 9) was provided under MTA from the Lee lab (Nationwide Children's Hospital). AsPC1-Luc (AsPC1 gifted by Jan Grimm, MSKCC and retrovirally transduced with luciferase) was provided by the Daniyan Lab (MSKCC). COS-7 cells were obtained through a material transfer agreement (MTA) from S. A. Rosenberg (National Cancer Institute).The J8Zb2m-α-β- NFAT reporter cell line has been previously described by our lab. Raji and Nalm6 with stable nuclear localization sequence (NLS)-mCherry or NLS-GFP reporter expression were developed by retroviral transduction. K562-CD19 FASLG-KO were generated by CRISPR gene editing.
Authentication	All cell lines, including those generated in the lab, purchased from a commercial vendor, or received from another lab under MTA or as a collaboration, were authenticated by flow cytometry or Sanger sequencing.
Mycoplasma contamination	Negative.
Commonly misidentified lines (See ICLAC register)	No.

Animals and other research organisms

Policy information about studies involving animals; ARRIVE guidelines recommended for reporting animal research, and Sex and Gender in Research

Laboratory animals	Six to 10-week-old female NOD.Cg-Prkdcscid Il2rgtm1Wjl/SzJ (NSG) mice were used for all animal experiments (Jackson Laboratory) and housed in pathogen-free conditions at the MSKCC vivarium.
Wild animals	No.
Reporting on sex	Only female mice were used for in vivo experiments. However, there was no sex-linked models used in this study. Sex and gender were not considered in the study design and no analysis was used to determine sex difference.
Field-collected samples	No.
Ethics oversight	All mouse experiments were performed in accordance with an MSKCC Institutional Animal Care and Use Committee-approved protocol (19-08-013). Animal ethics oversight conducted by MSKCC IACUC and veterinary staff. The maximum tumor volume for solid tumors was set at 1000 mm3 with no exceptions and was not exceeded. Euthanasia was performed based on tumor volume limit or pre-determined clinical criteria including loss of >10% body weight, development of hind limb paralysis, hunched posture, labored breathing, scruffy coat, cage mate avoidance, and lethargy.

Note that full information on the approval of the study protocol must also be provided in the manuscript.

Plants

Seed stocks	*Report on the source of all seed stocks or other plant material used. If applicable, state the seed stock centre and catalogue number. If plant specimens were collected from the field, describe the collection location, date and sampling procedures.*
Novel plant genotypes	*Describe the methods by which all novel plant genotypes were produced. This includes those generated by transgenic approaches, gene editing, chemical/radiation-based mutagenesis and hybridization. For transgenic lines, describe the transformation method, the number of independent lines analyzed and the generation upon which experiments were performed. For gene-edited lines, describe the editor used, the endogenous sequence targeted for editing, the targeting guide RNA sequence (if applicable) and how the editor was applied.*
Authentication	*Describe any authentication procedures for each seed stock used or novel genotype generated. Describe any experiments used to assess the effect of a mutation and, where applicable, how potential secondary effects (e.g. second site T-DNA insertions, mosiacism, off-target gene editing) were examined.*

Flow Cytometry

Plots

Confirm that:

☒ The axis labels state the marker and fluorochrome used (e.g. CD4-FITC).

☒ The axis scales are clearly visible. Include numbers along axes only for bottom left plot of group (a 'group' is an analysis of identical markers).

☒ All plots are contour plots with outliers or pseudocolor plots.

☒ A numerical value for number of cells or percentage (with statistics) is provided.

Methodology

Sample preparation	For surface staining, cells were washed with PBS and stained with antibodies at 4°C for 30 min in PBS supplemented with 0.5% FBS. Cells were washed twice with PBS + 0.5% FBS and acquired on an LSRFortessa X-20 (BD). For NK cell staining, T cell FasL staining and mice tissue staining, Fc blocking antibody or Human TrueStain FcX blocking solution (Biolegend, 422302) was added to cells for 10 min before staining. Cells were washed twice with PBS + 0.5% FBS before acquisition or used for further staining. For intracellular staining, T cells or NK cells were mixed with tumor cells for 6 h in the presence of GolgiPlug (BD, BDB555029). As positive controls, either eBioscience™ Cell Stimulation Cocktail (500X) (Thermo Fisher, 00-4970-03) or phorbol 12-myristate 13-acetate/ionomycin (PMA/I) was added to an aliquot of cells during the incubation. After staining using surface antibodies and LIVE/DEAD, cells were permeabilized and fixed by Fixation/Permeablization Kit (BD, 555028) for 20 min at 4°C. Cells were then washed once in Perm/Wash buffer (BD, 51-2091KZ) and stained by antibodies for 40 min at 4° C. Cells were washed twice with Perm/Wash buffer before acquisition.
Instrument	BD LSRFortessa X-20.
Software	Flowjo 10.

Cell population abundance	Cell population abundance varies for in vivo samples. For in vitro assays, 50k to 1m cells per sample were acquired. For in vivo samples, Up to 1 million cells per sample were acquired.
Gating strategy	Gating hierarchy was provided in Supplementary Figures 1 and 2.

☒ Tick this box to confirm that a figure exemplifying the gating strategy is provided in the Supplementary Information.